

Accepted Manuscript

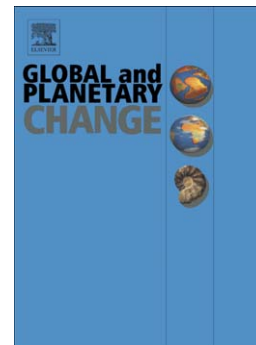
Control of sedimentation by active tectonics, glaciation and contourite-depositing currents in Endurance Basin, South Georgia

Matthew J. Owen, Simon J. Day, Philip T. Leat, Alex J. Tate, Tara J. Martin

PII: S0921-8181(14)00159-3
DOI: doi: [10.1016/j.gloplacha.2014.08.003](https://doi.org/10.1016/j.gloplacha.2014.08.003)
Reference: GLOBAL 2166

To appear in: *Global and Planetary Change*

Received date: 15 November 2013
Revised date: 19 March 2014
Accepted date: 1 August 2014



Please cite this article as: Owen, Matthew J., Day, Simon J., Leat, Philip T., Tate, Alex J., Martin, Tara J., Control of sedimentation by active tectonics, glaciation and contourite-depositing currents in Endurance Basin, South Georgia, *Global and Planetary Change* (2014), doi: [10.1016/j.gloplacha.2014.08.003](https://doi.org/10.1016/j.gloplacha.2014.08.003)

This is a PDF file of an unedited manuscript that has been accepted for publication. As a service to our customers we are providing this early version of the manuscript. The manuscript will undergo copyediting, typesetting, and review of the resulting proof before it is published in its final form. Please note that during the production process errors may be discovered which could affect the content, and all legal disclaimers that apply to the journal pertain.

Control of sedimentation by active tectonics, glaciation and contourite-depositing currents in Endurance Basin, South Georgia

Matthew J Owen^{a,*}

Simon J Day^b

Philip T Leat^{c,1}

Alex J Tate^c

Tara J Martin^{c,2}

a. Department of Geography, University College London, Gower Street, London. WC1E 6BT, UK

b. Department of Earth Sciences, University College London, 136 Gower Street, London WC1E 6BT, UK

c. British Antarctic Survey, High Cross, Madingley Road, Cambridge CB3 0ET, UK

1. Present address: Department of Geology, University of Leicester, University Road, Leicester LE1 7RH, UK

2. Present address: CSIRO National Marine Facility, Castray Esplanade, Hobart, Tasmania, Australia.

* Corresponding Author: m.owen@ucl.ac.uk

Abstract

Endurance Basin is an elongate broadly WNW-ESE trending basin located on the northern margin of the Scotia Sea, adjacent to the southern margin of the South Georgia micro-continent. Bathymetric and TOPAS sub-bottom profile data acquired in 2010 by the British research ship RRS James Clark Ross map this basin and its sedimentology for the first time. Endurance Basin contains a number of sub-basins and a substantial glaciogenic fan. The northern margin of Endurance Basin is formed by a series of steep slopes and intervening troughs. These are interpreted as a left-stepping en echelon array of oblique, strike-slip faults whilst the sub-basins are separated by compressional dip-slip faults. It appears that South Georgia is moving NW with respect to the basin. We interpret five seismic facies from TOPAS data, which are associated with distinct sedimentologies. The most striking units in the basin fill are: substantial contourite drifts located in the NW of the basin and on its southern margin; and two distinct mass transport deposits that pond in the centre of the basin. Combined with the known regional oceanographic setting, the contourites provide evidence of broadly eastward flowing bottom currents, entering the basin from at least two locations. Although landslide scars are present on the steep northern basin margin, the imaged mass transport deposits are interpreted to have been sourced from the glaciogenic fan, located in the SE of the basin, and from a contourite unit located on the basin's southern margin. Sediments from these events are transported at least 40 km. The contourite drift sequence is at least 100 m thick in the west of the basin and may contain a palaeoenvironmental archive of Antarctic Circumpolar Current (ACC) flow and the climate of South Georgia extending to the Pliocene. Such an archive would allow reconstruction of ACC flow through the Pleistocene glaciations and provide a means of linking ocean circulation and climate records in the sub-Antarctic Polar Front region.

Keywords:

Transpression, mass transport deposit, Scotia Sea, contourites, glaciation

1. Introduction

The continental slopes of the Antarctic continent and sub-Antarctic micro-continents preserve records of sediment transport and deposition related to ocean currents and slope instabilities during glacial-interglacial cycles (Dowdeswell et al., 2006; Noormets et al., 2009; Gales et al., 2012; Casas et al., 2013; Gales et al., 2013). South Georgia is the largest of the micro-continental blocks in the Scotia Sea (Figure 1.A). Because of its position in the northern Scotia Sea, and history of glaciations, deposits in the basin and on the continental slopes provide a unique opportunity to investigate the interactions between glaciosedimentary and oceanographic processes associated with the Antarctic Circumpolar Current (ACC) during glacial-interglacial cycles.

Situated between the Polar Front (PF) and the Southern Antarctic Circumpolar Current Front (SACCF) (Meredith et al., 2003), the proximal basins south of South Georgia represent an ideal and under-utilised location to investigate the palaeoflow of the ACC (Figure 1.B). This current transports >100 Sv eastwards and the deep water components exported from the Southern Ocean ventilate the majority of the world's oceans; it is, therefore, a key component of the global thermohaline system (Orsi et al., 1995; Orsi et al., 1999; Gebbie and Huybers, 2011). Improved knowledge of its variation will help understanding of the relative contribution of ocean circulation and greenhouse gases as climate influences (Barker and Thomas, 2004).

Although there is some debate surrounding the timing of the onset of the ACC, it is agreed that this is directly related to the deepening of the Drake Passage and the creation of a continuous circumpolar seaway. This has been widely proposed to have occurred around the time of the Oligocene-Eocene boundary at circa 30 Ma (Barker and Burrell, 1977; Barker and Thomas, 2004; Lodolo et al., 2006; Livermore et al., 2007). An alternative view is that a deep ocean gateway did not open until after the mid-Miocene climate optimum (Dalziel et al., 2013b). In both cases, rapid climatic cooling followed opening of the ocean gateway, associated with expansion and stabilization of Antarctic ice-sheets (Zachos et al., 2001). Variation has been noted in the intensity of ACC circulation during the Pleistocene, with stronger flow observed during glacials and weaker flow during interglacials (Pudsey and Howe, 2002).

Though it is primarily wind-driven, there are shallow and deep components to the ACC, which extend to the ocean floor (Pudsey and Howe, 1998; Orsi et al., 1999; Pudsey and Howe, 2002). This deep circulation, which entrains North Atlantic Deep Water (NADW) (Whitworth III and Nowlin Jr, 1987), is distinct from Antarctic Bottom Water (AABW) and its

components, which form on the Antarctic shelf-edge, are cooler and more dense (Orsi et al., 1999).

The climate of South Georgia, which is controlled by the position of the polar front and the intensity of westerly winds, has been subject to several investigations in recent years (Rosqvist and Schuber, 2003; Bentley et al., 2007; Van der Putten et al., 2009). However, these studies are mainly terrestrial in scope and confined to the Holocene and last deglaciation due to the erosive effects of ice-sheets on older palaeoenvironmental records. The presence of cross-shelf troughs and shelf-edge moraines supports a model of extensive ice-cover during past glacial history (the maximum ice extent during the last glacial maximum (LGM) is uncertain; Graham et al., 2008), which would have deposited sediments past the shelf-edge. Investigations of other glaciated, or formerly glaciated, margins have documented a number of features including fans of glaciogenic sediment, gullies, canyons and mass transport deposits (Dowdeswell et al., 1998; Dowdeswell et al., 2006; Noormets et al., 2009; Gales et al., 2012; Gales et al., 2013). Interaction between glaciogenic and contouritic sedimentation has also been documented on some continental slopes, providing a valuable archive and influencing slope stability (Knutz et al., 2002; Laberg et al., 2002; Bryn et al., 2005b; Solheim et al., 2005). If present around South Georgia, such interactions potentially provide records of the relationship between terrestrial glaciations of South Georgia and the regional ocean currents; in particular the ACC.

As such, the adjacent deep basins should contain a longer record of South Georgia's climate and oceanographic setting, as well as evidence of mass movement events triggered on the surrounding slopes. This paper documents and describes such a basin, using results of a geophysical survey to the south of the South Georgia micro-continent by the British research ship RRS James Clark Ross during January 2010. The proposed name for this feature, which may prove to be a valuable archive of palaeoenvironmental data for the sub-Antarctic, is Endurance Basin.

2. Regional Setting

2.1. Regional tectonic setting

South Georgia comprises continental lithosphere that rifted from southern South America during the opening of the Drake Passage between South America and Antarctica (Dalziel et al., 1975; Dalziel et al., 2013a). It is a micro-continental block that is situated within the North Scotia Ridge (Figure 1.A), a plate boundary that extends some 2000 km from South

Georgia to Tierra del Fuego (Cunningham et al., 1998). The North Scotia Ridge marks the position of a slow-moving sinistral transcurrent plate boundary along which the relative motion between the Scotia plate to the south and the South America plate to the north is about 7.1 mm yr^{-1} (Thomas et al., 2003). South Georgia is thought to be part of the Scotia plate and is situated in a restraining bend on the plate boundary (Thomas et al., 2003; Smalley et al., 2007). A cluster of earthquakes in 2002 (Figure 1.C) centred along the southern margin of the South Georgia continental block indicate that compression generated at the restraining bend is causing South Georgia to be thrust to the SW over the adjacent part of the Scotia plate (Thomas et al., 2003; Smalley et al., 2007; USGS, 2014). An earlier earthquake (1965) occurred beneath the upper continental slope adjacent to the Endurance Basin (Figures 1.C and 2). The focal mechanism of this earthquake also indicates thrusting of South Georgia to the SW over the crust of the Endurance Basin (Pelayo and Wiens, 1989; Thomas et al., 2003). In this scenario, the Endurance Basin in its present form, is a foreland basin formed by loading of the Scotia plate by uplift of South Georgia along the thrust system.

The nature of the lithosphere forming the basement to the Endurance Basin is uncertain. There are several models for the origin of the Central Scotia Sea, of which the Endurance Basin forms the northernmost part. Hill and Barker (1980) identified east-west-trending magnetic anomalies in the central part of the Scotia plate, which are clearly distinct from the north-south magnetic anomalies formed by well-understood ocean spreading in the West and East Scotia Seas (Barker, 1995; Larter et al., 2003; Eagles, 2005), and suggested that they were Miocene in age. Eagles (2010), by contrast, reinterpreted the Central Scotia Sea as a fragment of Mesozoic ocean lithosphere generated during separation of Antarctica from South America. Dalziel et al. (2013b) found evidence for an Oligocene-Miocene volcanic arc in the Central Scotia Sea and suggested that this overlies the Mesozoic ocean plate suggested by Eagles (2010).

2.2. Regional climatic and oceanographic setting

Being situated in the sub-Antarctic at approximately 55° S (Figure 1.B), South Georgia is at present approximately 5° northward of the average winter sea ice limit (Rosqvist and Schuber, 2003). However, based on studies of sediment core diatom assemblages, it appears that the winter sea ice limit extended north of South Georgia during the LGM (Gersonde et al., 2005; Allen et al., 2011; Collins et al., 2012). Bathymetric data reveal the presence of a number of across-shelf troughs and shelf-edge moraines, indicating repeat ice-sheet advance over the micro-continent's shelf (Graham et al., 2008). Today, half of

the island remains ice-covered by valley glaciers (Rosqvist and Schuber, 2003; Gordon et al., 2008).

South Georgia is situated between the polar front, to the north, and the ACC front to the south. The North Scotia Ridge acts to constrain the ACC flow, providing a barrier to the deep water components (Orsi et al., 1995; Smith et al., 2009). Shag Rocks Passage (SRP) is an exception to this, allowing a proportion of the water mass to flow north of South Georgia, therefore, moving the polar front further north (see Figure 1; Thorpe et al., 2002; Smith et al., 2009). Supporting this, Howe et al. (1997) document contourite units, indicative of strong current flow at 3000 m water depth in the west Falklands Trough. In addition to this, Weddell Sea Deep Water (WSDW) has been interpreted to flow north into the Central Scotia Sea (Pudsey and Howe, 1998; Maldonado et al., 2003; Meredith et al., 2008; Lobo et al., 2011) at which point it may merge with the deep components of the ACC. This merging is likely to occur not far south of South Georgia, further enhancing the palaeoceanographic significance of the region's basin sediment records.

Holocene sediments in the North Scotia Sea are dominated by foraminifera bearing (carbonate preservation is poor) diatomaceous oozes, with rare ice-rafted debris (IRD) from the eastern margin of the Antarctic Peninsula (Pudsey and Howe, 1998). During the LGM the situation changes, with diatomaceous mud and a greater proportion of IRD from more numerous sources, including: both east and west margins of the Antarctic Peninsula, southern South America and some of the sub-Antarctic islands including the South Orkneys and the South Shetlands (Sugden and Clapperton, 1977; Pudsey and Howe, 1998).

3. Material and methods

Data were acquired between the 21st and 29th of January 2010 on cruise JR206 (NERC Cruise leg JR20100118) of British research ship RRS James Clark Ross. Bathymetric data were acquired using a hull-mounted Simrad EM 120 multibeam echo sounder. The system had a 12 kHz operating frequency and a 191 beam array with real-time beam steering and active pitch and roll compensation (Tate and Leat, 2007; Leat et al., 2010). Data were acquired using Simrad's Merlin software and were cleaned manually using MB System v5.0.9 software. Cleaned data were gridded at 100 m horizontal resolution. Vertical measurement accuracy is in the order of 50 cm or 0.2% of depth RMS (de Moustier, 2001)(whichever is greater). At 3500 m water depth, this corresponds to an accuracy of 7 m. This new data was combined with that from previous transits in the area (see list of data sources in Table 1).

Sub-bottom data were collected using a hull-mounted Simrad TOPAS PS 018 profiler. All runs were made using chirp mode on 90% power with a pulse length of 15 ms and start and stop frequencies of 1.5 and 5.0 kHz respectively. A total of 647 km of sub-bottom lines were acquired (Table 2 and Figure 2), vessel speed varied between 6 and 10 knots, and ping interval was generally 2 s, except when run concurrently with the EM 120 when the interval was increased to 7 s to reduce interference. A matched filter operating between 1.0 and 5.5 kHz was applied to the data offline in TOPAS replay. Processed data were exported as SEG Y before being converted to COD and interpreted in Survey Engine™ Seismic+™ from CodaOctopus.

Deposit thickness estimates and isopach maps were derived from the TOPAS lines via a spline of interpreted sub-bottom points. However, they have been forced to zero values at the base of the steep northern and southern margins, between TOPAS lines, where seismic data indicate that the units pinch out. No forcing of values has been performed on the western limit of the data, where bathymetry and sub-surface geology is poorly constrained.

All maps are plotted in the WGS 1984 UTM 24 South projection, though some are rotated to provide the most appropriate view.

4. Results and TOPAS interpretation

4.1. Bathymetric mapping

Figures 2 and 3 show detailed bathymetry located south of South Georgia. The new multibeam sonar data, combined with swaths of multibeam data from previous passages, produced a near-complete bathymetric map of the elongate, broadly WNW-ESE trending Endurance Basin. The basin is around 160 km long and 20 - 50 km wide, between approximately 54.3° S, 39.7° W and 55.3° S, 38.0° W. Its long axis is approximately parallel to the continental margin, with a well defined NE margin but a less well defined SW margin.

4.1.1. *Basin morphology*

Basin parameters are summarised in Table 3. The northern margin of the Endurance Basin is formed by a series of steep slopes and intervening troughs rising some 3000 m to the shelf edge (Figure 2). Individual slope segments trend slightly oblique to the basin and are linked by SE-facing ramps and slopes. Where they intersect the basin floor, some of the main scarps curve into subtle N-S trending scarps and ridges that divide the basin into at least three sub-basins with nearly flat floors and slightly different bathymetric depths.

The southern margin of the basin consists of a series of en echelon scarps up to a few hundreds of metres high that are also left-stepping and linked by E-W trending scarps. The WNW end of the mapped basin steps south-westward into further, slightly shallower water depth basins. The eastern end of the basin is bounded by a scarp and fan (with an area of at least 620 km²) system at the mouth of a canyon cutting the micro-continent margin. The canyon coincides with the only shelf trough, interpreted as the pathway of an ice stream, to be identified on the south side of the micro-continent by Graham et al. (2008). The northwestern side of the fan is cut by a channel and canyon system inferred to be the currently or most recently active sediment pathway from the shelf to the basin, whereas the crest of the fan is occupied by a topographically subdued channel system that is inferred to have been abandoned.

4.1.2. *Mass transport scars*

The northern margin of Endurance Basin is marked by three scarps that are interpreted to have formed as a consequence of slope failure events (Figures 2 and 3). The largest of these is 50 km² in area and displays gradients of up to 37°. The smaller scarps have steeper gradients, reaching 49°. Some possible associated debris deposits or slide blocks may be present downslope from the scarp located at 54.79° S, 38.87° W (see Figure 3.C), though this irregular bathymetry may be associated with the nearby scarp slopes and TOPAS data is inconclusive. Otherwise no debris or blocks were identified on the basin floor from the bathymetric data, suggesting that the scarps are relatively old with deposits that are buried beneath basin-floor sediments, or that the mass flows consisted of disaggregated debris that are not easily distinguishable in the TOPAS profiles.

In addition to these clear, relatively small, scarps there is also a less well defined, broad and more gently angled embayment on the basin's southern margin (location indicated on Figure 2). This has an area of circa 120 km² and contains a prominent pinnacle feature with a relief of >300 m and gradients of up to 30°. A noticeable annular depression, open to the northeast, surrounds this feature. Slopes within the embayment dip to the northeast and are generally <2°, though they are greater on the margins where they reach 7°.

4.2. TOPAS data

4.2.1. *Description and characteristics of seismic facies*

Figures 4 to 8 show a NW to SE transect along the axis of Endurance Basin (see Figure 2 for location of profiles). Key features within this transect are shown in greater detail in Figures 5 and 7. Sub-surface penetration varied between 130 ms Two-Way-Travel-Time

(TWTT) in the northwest of the basin and practically no penetration on parts of the glaciogenic fan in the southeast.

TOPAS line 17 (Figure 4) shows a 55 km long profile located at the western end of Endurance Basin. The start of the line, in the far west, reveals a relatively rugged seabed with steep slopes and no seismic penetration. Between fix markers 2 and 4 the seabed becomes smoother and the line crosses a number of seabed undulations, which display increased penetration, showing closely spaced parallel reflectors. Figure 5.A shows a trough between these crests in more detail. From this detailed imagery it can be seen that parallel near surface reflectors are underlain by more chaotic and deformed units. A number of possible faults are observed, though this apparent displacement could also indicate irregular surfaces formed via mass transport deposits (MTDs).

Beyond the area of undulations, the sub-surface penetration increases dramatically from ~20 ms TWTT to ~130 ms TWTT, showing a thick laminated sub-parallel sequence of reflectors that extend 15 km across the basin floor. These reflectors become more closely spaced in the east, where they eventually pinch-out and onlap the basin's northern margin. In the east, deeper sections of this sequence lose structure and may be folded. Figure 5.B shows this section in greater detail.

The eastern end of TOPAS line 17 traverses the lower section of the basin's northern margin where there is little or no seismic penetration. However, a number of features are apparent, notably a succession of tilted blocks, which may indicate faulting.

TOPAS line 7 (Figure 6) crosses the centre of Endurance Basin with a 62 km long profile and intersects TOPAS lines 11 and 12 (shown in Figures 9 and 8 respectively). Moving west to east, a marked change in seismic facies is observed, with limited penetration in the west revealing plane-stratified reflectors; and a ponded sequence of units visible towards the east of the line in the centre of the basin.

These two regions are separated by an elevated structure (termed block A), interpreted as a block uplifted along a cross-basin fault pair (see section 5.1 and Figure 13.A). An additional fault is interpreted approximately 2.5 km downslope from block A (shown in detail in Figure 7.A). Immediately upslope, to the west of block A, sediments appear to accumulate in a convex up geometry, which we infer to indicate a mounded deposit when considered in 3D. Further east a possible anticline is visible near fix marker 11, just before a 2.8 km data gap.

The ponded sequence of units extends over a distance of some 40 km to the southeastern end of TOPAS line 7. The uppermost unit is largely transparent and reaches a thickness of 15 ms TWTT in the centre of the basin. However, the unit's maximum thickness of 21 ms TWTT is observed at the eastern end of TOPAS line 7 where a steep sided, elevated geometry is displayed over a distance of 9 km. There is no visible reflector separating this feature from the rest of the unit.

Below this transparent unit is a higher amplitude, chaotic, ponded unit, which appears to erode the stratified unit beneath it again (see Figure 7.B). Within TOPAS line 7, this unit reaches a maximum thickness of 20 ms TWTT.

These two ponded units rest above a sequence of alternating stratified and transparent units, which thicken towards the centre of the basin.

A 30 km section from TOPAS line 12, running between the centre of the basin and the lower section of the glaciogenic fan, is displayed in Figure 8. The two ponded units identified in Figure 6 are again apparent and the units within TOPAS lines 12 and 7 correlate at their intersection. Overlying these units, an additional thin, lens-like unit is visible towards the west of the line. Seismic penetration is dramatically reduced on the glaciogenic fan's lower slopes at the eastern end of the line.

The transparent upper ponded unit thins to eastward, reaching a minimum thickness of 9 ms TWTT, before thickening to 16 ms TWTT adjacent to the toe of the fan. The unit then onlaps the fan surface.

The basal reflector of the lower chaotic, ponded unit (below the upper transparent unit) can be traced for some 6.5 km east from the start of TOPAS line 12. Within this section the unit is observed to thicken significantly. Moving eastward the unit's upper boundary forms an asymmetric, irregular, elevated deposit (of 20 km length) and severely limits seismic penetration; making identification of unit thickness impossible. An area of more transparent chaotic facies is observed between this elevated unit and the toe of the fan to the east.

There is practically no seismic penetration from TOPAS data on the fan. However, the TOPAS data provides a useful additional source of information on the area's seabed morphology. The fan's lower slope is convex up before gradients increase and the fan continues upslope to a canyon system linking it to the micro-continental shelf (Figure 8).

Whereas Figures 4 - 8 presented a west to east transect through the basin, TOPAS line 11 (Figure 9) shows a 16 km south to north profile between the southern and northern margins. The southern section of the line presents similar data to Figures 6 and 8, with the

same units apparent. The thin, lens-like surface unit visible in Figure 8 is observed slightly north of the line's intersection with TOPAS line 12. The upper transparent unit is less obviously ponded than in TOPAS lines 7 and 12, though it does thin slightly to the north. The lower chaotic unit thickens notably in the centre of the basin.

As shown by the bathymetry, and reinforced by the TOPAS data, the northern margin is extremely steep and appears irregular, with numerous hyperbolae. It is unclear whether mound-like facies situated immediately south of the slope break are real (in which case they probably represent debris sourced from the slope) or artefacts caused by side-swipe from prominent bathymetry.

North from the slope break TOPAS line 11 crosses a smaller basin, which contains stratified sediments, situated between interpreted fault scarps. The northernmost section of TOPAS line 11 is not shown as the steep slopes contain little data of use, save a verification of the absence of thick sediments.

Traversing the basin's southern margin, a section of TOPAS line 9 is shown in Figure 10. The eastern section of the line reveals parallel laminated reflectors, which pinch out in a channel located adjacent to the prominent pinnacle observed in bathymetric data (Figure 2). Seismic penetration is then minimal and the line appears to cross a steep scarp.

On the basis of the reflectivity and geometry of the surface and sub-surface sediments we interpret five distinct seismic units, which are summarised in Figure 11 and indicated on Figures 4 to 10. Expanding the morphological facies concept originally developed for debris avalanche deposits by Glicken (1996), units III and IV are divided into morphological facies a and b. This division is based on Glicken's observation that deposits from the same mass transport event show lateral variation and may display different morphologies. Faults are identified via vertical displacement of reflectors and occasional loss of sedimentary structure. Origin and mechanistic interpretation of these units are discussed in section 5.2.

4.2.2. *Thickness of units*

Figure 12 presents an isopach of units III and IV. These are expressed in metres, assuming a seismic velocity of 1600 m s^{-1} , which is appropriate for shallow sediments in high latitudes (Schlesinger et al., 2012). It is possible that the deeper unit III may in reality have a greater velocity, but in the absence of information a single depth conversion is used.

Figure 12.A shows the interpreted thickness of seismic unit IV. From a thickness of 12 m in the centre of the basin, the unit thins gradually to the west. The thickest occurrences (maximum thickness is calculated as 17 m) are associated with the elevated deposits of the IVa morphological facies shown at the eastern end of Figure 6. Thickness increases in depressions in the eastern part of the basin, before the unit thins rapidly as it onlaps the glaciogenic fan. This unit's estimated volume is 4.2 km³.

Thickness of seismic unit III is shown in Figure 12.B. This unit reaches a maximum interpreted thickness of 24 m where the IIIa morphological facies ponds near the basin's northern margin. The unit thins gradually to the west, where it onlaps the underlying stratified units (shown in Figure 6). It was not possible to calculate thickness towards the east of the basin due to insufficient seismic penetration, however the unit is believed to be present west of the glaciogenic fan. The unit's calculated volume (which represents an incomplete volume) is 3.3 km³.

Isopachs were not created for seismic units I, II and V due to insufficient data. However, by way of illustration, if a seismic velocity of 1600 m s⁻¹ is assumed, then seismic unit I has a maximum observed thickness of 25 m, unit II has a thickness of at least 100 m (though the unit extends beyond the limit of seismic penetration) and unit V a thickness of up to 2.5 m.

5. Discussion

5.1. Tectonic origin of the basin

Fault patterns observed in the multibeam and TOPAS data (Figures 2, 4, 5, 6 and 7) indicate that the margins of the basin are strongly fault-defined. The regional plate tectonic setting (Figures 1.A, 13.A; Thomas et al., 2003; Smalley et al., 2007) implies that these faults developed in a transpressive left-lateral tectonic regime.

Supporting evidence for crustal down-warping associated with overthrusting of South Georgia onto the Scotia Sea plate can be seen in satellite-derived gravity free-air anomalies which show a pronounced low of -80 mGal over the basin (Livermore et al., 1994; Eagles, 2010). Earthquake focal mechanism data (Pelayo and Wiens, 1989; USGS, 2014) demonstrates that the southern margin of the South Georgia lithosphere is being thrust SW over the Central Scotia Sea part of the Scotia plate. This suggests that the Endurance Basin is a foreland basin that developed along down-flexed lithosphere in the footwall adjacent to the overthrust continental margin.

New data presented here display substantial evidence of faulting. The slope segments, in the basin's northern margin, trending obliquely to the basin are interpreted as a left-

stepping en echelon array of oblique, strike-slip fault scarps with intervening elongate highs and small basins (Figure 2 and 13.A). North to south trending across-basin scarps appear to develop, and curve away, from the main faults within the northern margin. These N-S features, which divide Endurance Basin into the three sub-basins (Table 3 and Figure 13.A), are interpreted as reverse faults and compressional fault arrays. TOPAS line 7 crosses one of these structures, which is labelled Block A (Figure 6 and 13.A). Further supporting evidence of this interpretation is shown in TOPAS line 17 (Figure 4), where a number of tilted blocks are observed on the flank of the basin's northern margin. Possible deformation of deeper sediments imaged in TOPAS line 17 (Figures 4 and 5) adds further support to this compressional tectonic interpretation. The fault imaged in Figure 7.A, east of Block A, shows a clear vertical offset, but due to the TOPAS data resolution its dip is uncertain.

However, the geometry requires that N-S faults (Figure 6 and 7) crossing the basin and linking to the northern margin faults are compressional structures and likely high angle reverse faults. This geometry is also consistent with a component of left-lateral geometry of strike-slip faulting along the margin, as South Georgia and the shelf trough are moving NW with respect to the basin and the fan. En echelon scarps observed on the basin's southern margin (Figure 2 and 13.A) are interpreted as normal faults, being orthogonal to the basin-crossing compressional ridges.

Relatively recent development of Endurance Basin as a mainly compressive feature may be superimposed on an earlier dextral strike-slip fault system, along which South Georgia was translated to the east relative to the South American plate to the north as it was rifted from Tierra del Fuego (Dalziel et al., 1975). Therefore, it may have undergone one or more periods of inversion between the initial opening of Drake Passage and the present, with South Georgia initially moving east relative to South America with the Scotia plate but subsequently being partly transferred to South America and so moving west relative to the Scotia Sea on the SW-directed thrust faults.

Similar continental margin-parallel marginal basins associated with local transpression and negative free-air gravity anomalies are observed along the northern margin of the sinistral South Scotia Ridge west of the South Orkney micro-continent (Galindo-Zaldívar et al., 1996; Bohoyo et al., 2007; Lodolo et al., 2010). However, in general features identified on the South Scotia Ridge have a greater association with transtension (Galindo-Zaldívar et al., 1996; Bohoyo et al., 2007; Lodolo et al., 2010; Civile et al., 2012) than the left-lateral transpression documented on the northern margin of Endurance Basin in this paper.

Looking further afield, analogies for the development of Endurance Basin may be found on the broadly strike-slip northern and southern boundaries of the Caribbean Plate, especially in the basins on the southwest side of Hispaniola. Hispaniola has in the past extended as it moved east with the Caribbean plate but is now experiencing transpression as it is being transferred progressively to the North American Plate and so moves west relative to the Caribbean, shortening and deepening the basins on its southwest side as they are overthrust by crustal blocks forming central Hispaniola (Mann et al., 1991; Pubellier et al., 2000).

5.2. Inferred origin of interpreted seismic facies

Depositional and transport processes of sedimentary units may be interpreted on the basis of their reflective characteristics and geometry (Piper et al., 1999). As such, we now consider the characteristics of interpreted seismic facies (Figure 11) and whether they are indicative of a particular sedimentology.

Seismic unit I consists of stratified, parallel reflectors and allows limited seismic penetration. The unit seems to drape underlying strata. Data coverage of this unit is relatively sparse and the interpreted origin is uncertain. However, on the basis of the reflective characteristics and location of the interpreted facies within Endurance Basin, it is considered that this unit is most likely to consist of hemipelagic material, with possible down-slope input from the basin margins. The unit may be influenced by bottom currents, with reduced seismic penetration potentially due to the presence of coarser sediment.

5.2.1. *Contourites*

The geometry of seismic unit II is typical of a type of contourite drift (Faugères et al., 1999; Maldonado et al., 2003; Maldonado et al., 2005; Faugères and Stow, 2008). Contourite deposits, which form under the influence of contour parallel currents, display a variety of forms that reflect variation in current velocity, sediment supply and seabed morphology. Typical seismic characteristics of contourites include: wavy, continuous, parallel to sub-parallel reflectors that converge towards the margins of the depositional bodies (Faugères et al., 1999; Maldonado et al., 2005). Contourite deposits may also display distinctive morphologies that are visible in bathymetry, for example elevated, elongate mounds and eroded moats and furrows (Maldonado et al., 2005; Howe et al., 2006; Lobo et al., 2011).

In particular, the sigmoidal geometry displayed in TOPAS line 17 (Figure 4) is similar to the slope plastered drifts interpreted by Pudsey and Howe (2002) and Maldonado et al. (2003) in the Central Scotia Sea. Though, the bathymetric setting and observed mounded morphology is comparable to mounded drifts described by Maldonado et al. (2005). The

eastward convergence of reflectors (Figure 5.B) may reflect a concurrent increase in bottom current velocity, reducing the sedimentation rate. Indications of current scour further southeast in Endurance Basin (for example the annular trough around the prominent pinnacle to the south of the basin, shown in Figure 10) provide further evidence of sediment deposition and erosion under the influence of accelerating bottom currents in a manner similar to that observed in other channel-like environments (Dorn and Werner, 1993; Marani et al., 1993; Howe et al., 1997; Llave et al., 2006).

Summarised in Figure 13.B, bathymetry and TOPAS data provide strong evidence of contourite deposits within Endurance Basin. In turn, these deposits indicate the presence of bottom currents flowing through Endurance Basin and its adjacent slopes implying the presence of ACC and/or WSDW flowing west to east to the south of South Georgia.

The thickest accumulation of the well-stratified unit II documented in this study is located in the northwest of Endurance Basin and shown in Figure 4. Here the unit is at least 130 ms TWTT (104 m assuming a seismic velocity of 1600 m s^{-1}) thick, though the base extends beyond the limit of seismic penetration. This unit thins towards the basin's northeastern margin where bathymetric depths increase. As contourites tend to accumulate thicker deposits in areas of reduced current velocity (Faugères and Stow, 2008) this geometry, consistent with the known oceanography of the Northern Scotia Sea (Orsi et al., 1995; Thorpe et al., 2002; Meredith et al., 2008; Smith et al., 2009), supports the presence of a bottom current flowing southeastwards along the base of the South Georgia micro-continental slope.

Additional occurrences of seismic unit II are observed on Endurance Basin's southern margin west of 38.7° W and are shown in Figure 10. As imaged in TOPAS lines 8 and 9, the unit pinches out at a horseshoe-shaped feature surrounding the base of the prominent pinnacle (Figure 10), providing possible evidence of an additional bottom current pathway into the basin.

5.2.2. *Mass transport deposits*

Seismic unit III displays two distinct morphological facies. Shown in Figure 8, Unit IIIa displays a chaotic, irregular and elevated geometry and is coupled with a possible slump at the toe of the glaciogenic fan (further north, TOPAS line 19 also indicates a similar convex up deposit at the toe of the fan). The chaotic upper unit IIIa pinches out in the west and masks deeper strata.

The chaotic, ponded morphology of unit IIIb is very similar to units that have been interpreted as debris flow deposits by other authors (Piper et al., 1999; Canals et al., 2004;

Tripsanas et al., 2008; Dondurur et al., 2013). Diagnostic seismic characteristics of these deposits include chaotic, transparent to semi-transparent seismic facies with a lack on internal structure (Canals et al., 2004). Ponding of deposits results from gravity acting on the mobile sediment, forcing particles into depressions. This effect may be magnified for fine grained cohesive sediments (clays) where electro-chemical bonds between particles may result in back-draining into basinal lows (Talling et al., 2012).

We, therefore, suggest that the observed morphology of unit IIIb results from the disintegration and gravity driven accumulation of sediments within depressions. The chaotic nature of the facies supports a disintegrative, rather than coherent, transport mechanism, such as has been documented on lower slopes at Trænadjupet, offshore Norway, by Laberg and Vorren (2000). The apparent erosion of underlying strata shown in Figure 7.B provides further support for emplacement via mass transport.

On the basis of these observations it seems likely that a slump and/or debris flow originated on the fan and transporting sediments westward, evolving as it did so, to produce the two distinct morphological facies in the sense defined by Glicken (1996). Unit IIIa deposits shown in Figure 8 representing the proximal, cohesive, high basal friction component and unit IIIb (Figures 7 and 9) representing the more distal deposits.

Originating on the glaciogenic fan, we speculate that this deposit may be related to overburden as a consequence of rapid sedimentation as the South Georgia micro-continent's ice-sheet retreated from the shelf (Graham et al., 2008).

The morphology of unit IV is different to unit III: being more transparent and less obviously ponded. As such, consideration was given to whether the apparent thinning and onlap of unit IV is caused by sedimentation rate changes and/or later erosion due to bottom currents. Interpreted contourite deposits (section 5.2.1) provide evidence of significant bottom current activity in Endurance Basin and the lack of seismic penetration on the glaciogenic fan and west of Block A (Figures 8 and 13.A) could indicate winnowing of fine material, as observed in other locations with vigorous bottom currents (McCave et al., 1995; Øvrebø et al., 2006; Preu et al., 2013). In this alternative interpretation, the transparent seismic unit IV could then represent a muddy contourite deposit, accumulating due to reduced current velocity and thinning on highs that experience increased flow rates (Stow and Faugères, 2008).

However, this alternative interpretation does not explain the elevated deposits within the unit and there are no obvious indications of current flow (i.e. moats, drift deposits or unit

asymmetry) in locations adjacent to the deposition of unit IV. Therefore we suggest that a debris or density flow origin is more likely.

We also divide the largely transparent seismic unit IV into two morphological facies (Glicken, 1996): unit IVa, the irregular, elevated facies and unit IVb, the smooth, ponded deposit that onlaps the underlying units (demonstrated in Figures 6 and 8). There is no obvious reflector separating the elevated feature from the ponded unit and it seems that they are two distinct morphologies of the same unit.

The elevated and irregular morphology of unit IVa, visible at the eastern end of Figure 6 and which extends for 9 km, provides a relative elevation of 5 m, is striking and bares marked similarity to debris flow deposits (Amy et al., 2005; Iverson et al., 2010). This positive morphology, which may indicate a cohesive debris flow (Tripsanas et al., 2007), contrasts the apparent lack of internal structure and smooth surface of unit IVb. This deposit is not visible in the bathymetric data, probably because the 5 m elevation is at the limit of the data's vertical accuracy at this depth (see Section 3).

Unit IVa is not visible on TOPAS lines 12 or 18, which are situated further north in the basin. However, it is visible in the northern section of TOPAS line 8, which extends southwards from TOPAS line 7 (Figure 2). A drift sequence is interpreted upslope from this location (Figures 10 and 13.B), which appears eroded in a section of TOPAS line 9, which traverses east to west across the basin's southern margin.

This erosion, characterised by converging reflectors, unit pinch out and possible stratigraphic truncation, at the western end of the drift, appears to be due to the action of bottom currents (as observed in the Falklands Trough by Howe et al. (1997)) and not as a result of sediment failure. However, the steep slope (20° - 30°) encountered 3.5 km to the west of the drift (Figure 10) trends north to south: apparently perpendicular to the direction of current flow inferred from the drift termination. As features eroded by bottom currents tend to form parallel to the direction of flow (Marani et al., 1993; Howe et al., 2006; Elliott et al., 2010; Preu et al., 2013), we suggest that the N-S trending steep slope is not a product of current erosion.

Although TOPAS line 9 (Figure 10) does not pass directly over the pinnacle, a relatively wide fresnel zone (~200 m in 3800 m water depth) means that this slope is probably associated with the pinnacle's northern buttress. However, bathymetric data (Figure 10.A) also shows a significant scarp slope trending north from the pinnacle for at least 2 km, with gradients reaching 20° . This slope may mark a headwall scar associated with the unit IVa deposit interpreted in TOPAS line 7 (Figure 6).

It appears that unit IVa, which is only observed adjacent to Endurance Basin's southern margin is sourced from the embayment located on the southwestern margin (indicated on Figure 2). Although, in this location slope angles are generally $<2^\circ$, on its margins they are appreciably steeper and submarine mass failures have been documented on slopes as low as 0.01° (Coleman et al., 1998; Walsh et al., 2006). Additionally, numerous large slides and slumps have been documented on submarine slopes with gradients in the order of 2° (see Owen et al., 2007 and references cited therein).

The 120 km^2 area of the embayment is consistent with the estimated 4.2 km^3 volume of unit IV and would require displacement of sediments 35 m thick to form the deposit. Not sourced from the glaciogenic fan, it seems likely that the event represents the failure of a contourite sequence in a manner previously observed in other high latitude locations (Bryn et al., 2005a; Elliott et al., 2010).

The prominent pinnacle visible in Figures 2 and 10 is intriguing and may exert influence on bottom current flow and sediment deposition. Bottom current flow is strongly influenced by interactions with bathymetric features that may cause changes in bottom current velocity and lead to turbulence and eddies (Alendal et al., 2005; Øvrebø et al., 2006). Such effects are noted elsewhere, for example at Rosemary Bank in the North Atlantic (Howe et al., 2006) and in the Plata del Mar Canyon on the Argentine margin (Voigt et al., 2013): in these locations changes in bottom current flow strongly influence sedimentation.

It is therefore plausible that this pinnacle, with a vertical relief of $>300 \text{ m}$ and surrounded by a horseshoe shaped depression (Figure 10.A), acts to focus bottom current flow: increasing adjacent current velocity, reducing sedimentation rates and causing the erosion visible in TOPAS line 9 (Figure 10.C). Once beyond the bathymetric constriction flow rates would decrease and allow greater rates of sedimentation: as observed in the Plata del Mar Canyon and on the Porcupine slope (Øvrebø et al., 2006; Voigt et al., 2013). We propose that this process may pre-condition the down-current slope to failure via increased sedimentation of fine material and possible undercutting of the deposited material by the adjacent current stream, in a manner similar to that suggested for the Rockall Bank Mass Flow by Elliot et al. (2010).

We emphasise that the different morphological facies of units III and IV represent different evolutionary stages of single mass movement events. We infer that the elevated deposits (IIIa and IVa) formed earlier in the mass movement process and are less disintegrated than the distal, onlapping deposits (IIIb and IVb) that may have become more fluidised or that may indicate deposition via a density flow (Hampton et al., 1996; Mulder and

Alexander, 2001; Mulder et al., 2003; Talling et al., 2012). The less pronounced ponding observed in unit IVb compared to unit IIIb may reflect particle size (and/or mineralogy) composition influencing sediment cohesion (Talling et al., 2012), or it may simply reflect the reduced seabed relief following deposition of unit III. We interpret unit IV as a debris flow or density flow deposit. The less pronounced ponding of the unit may indicate a less cohesive event than unit III. Sediment samples and more sub-bottom data are required to fully understand the unit.

Overlying the transparent unit IV, the lens-like seismic unit V appears to display a similar morphology, with margin pinch-out, to the surface debris flows documented by Iverson et al. (2010) and debrite deposits by Amy et al. (2005). The unit is thickest in TOPAS line 12 (Figure 7) and appears less pronounced in TOPAS line 11 (Figure 8), it is not apparent to the north of the basin in TOPAS line 18. As such, it seems most likely that the unit represents a small debris flow sourced from the basin's southern margin. It is not imaged in TOPAS line 7 as its apparent location would appear to correspond to the 2.8 km data gap (Figure 6).

5.3. A potential palaeoenvironmental archive?

As shown in Figure 4, unit II in the western part of the basin is clearly stratified throughout the imaged thickness. The sub-parallel reflectors appear to demonstrate the presence of a cyclic laminated sediment sequence at least 100 m thick (though the sequence extends beyond the limit of TOPAS data). Reflectivity in TOPAS line 17, shown in Figures 4 and 5.B, alternates between high and low amplitude, potentially indicating a concurrent alternation between coarse and fine material resulting in a succession of seismic impedance contrast changes. A further increase in reflectivity is observed in the deepest third of the imaged sequence, possibly indicating a significant change in the sedimentation regime, or diagenetic front, at this point (Figure 5.B). Changes seismic reflectivity (and particle size) may be caused by a number of factors, including: bottom current velocity variation (McCave et al., 1995; Øvrebø et al., 2006); changes sediment provenance (Rothwell et al., 1998; Hemming, 2004); porosity and density variation (Goff et al., 2004); and diagenetic modification of opal-A to opal-CT (Volpi et al., 2003). The clear stratification visible in TOPAS line 17, combined with the sedimentological and geochemical control of seismic reflectivity, suggests that unit II may contain important palaeoenvironmental records.

Sedimentation rates vary by orders of magnitude throughout the oceans and estimating rates accurately without sediment samples is impossible. However, it is possible to present

some tentative sedimentation rate ranges based on studies from the region and other similar deposits. Pudsey and Howe (1998) document sedimentation rates between 3.2 and 17 cm ka⁻¹ in the Scotia Sea since the LGM. Maldonado et al. (2003) estimate a rate of 2.7 cm ka⁻¹ for their seismic unit I, which represents late Pliocene to Holocene deposition in the Central Scotia Sea. Contourite drifts may yield appreciably higher sedimentation rates than these Scotia Sea studies show, with significant variation between glacial and interglacial periods also noted. For example, using radiocarbon dating, Knutz et al. (2007) constrain rates between 70 and 20 cm ka⁻¹ within sediment core DAPC2 in a contourite drift located in the Rockall Trough. It is, therefore, not safe to assume constant sedimentation rates.

Using the Scotia Sea sedimentation rate ranges calculated by Pudsey and Howe (1998), and an assumed seismic velocity of 1600 m s⁻¹ (this may be an underestimate, as seismic velocity is anticipated to increase with depth related compression), it seems probable that the drift sequence in the west of Endurance Basin should contain a record of sedimentation for at least the past 500 ka and potentially >3 Ma. However, it is impossible to verify the age of this sequence without drill sampling. As such this sequence is expected to contain a valuable archive of oceanographic, climatological and productivity data covering, at a minimum, the late Pleistocene glacial cycles and potentially extending into the Pliocene.

5.4. Overview of basin sedimentation

Broadly speaking, and indicated in Figure 13.B, Endurance Basin may be divided into four distinct sedimentation regimes: contourite drifts; plane stratified hemipelagic sequences; ponded debris or mass flow deposits; and the glaciogenic fan. This arrangement results from interaction between sediment sources and pathways and the regional tectonics; with a number of sub-basins formed between the N-S trending cross basin faults (Figure 13.A).

The contourite drifts in the west of the basin and on the southern margin (Figure 13.B) provide evidence of the eastward flowing bottom current, which may comprise both ACC and WSDW components (Pudsey and Howe, 1998; Thorpe et al., 2002; Maldonado et al., 2003; Meredith et al., 2008; Smith et al., 2009). Indeed the abyssal water mass of the western Endurance Basin may be distinct from that in the east.

The central area of Endurance Basin is characterised by a sequence of ponded units, which seem to be interdigitated with the stratified deposits (Figure 6). We have interpreted three seismic facies in this area, which on the basis of the TOPAS data, appear to have different source locations. Divided into two morphological facies, it seems that Unit III was

sourced from the glaciogenic fan and transported material westward into the centre of Endurance Basin. Overlying this unit, Unit IV appears to have been sourced from the contourite deposits on the southern margin. Unit V also seems to have been transported from the southern margin, though its origin is less obvious. At present no sediment samples have been acquired from Endurance Basin. Such data would be of great benefit in fully understanding the basin's sedimentology.

Currently there is insufficient evidence to consider slope failure susceptibility or trigger mechanisms. However, it seems plausible that unit III may be related to (de)glacial sedimentation and that located in an active tectonic region a seismic trigger is at least possible (Figure 1.C; Pelayo and Wiens, 1989; Thomas et al., 2003; Graham et al., 2008; USGS, 2014). If so, the implication is that the South Georgian continental slope landslide scars (Figure 3) pre-date the last glacial. How the prominent pinnacle, located in the interpreted source area of unit IV, influences local sedimentation and whether it affects slope stability is a question for future research.

The fan in the far southeast of Endurance Basin is inactive at present, and would appear to be active only during periods of ice-advance onto the micro-continent's shelf (Graham et al., 2008). The far southeastern margin of Endurance Basin is not mapped (Figures 2 and 13) and, as such, the sedimentology of this location is not known.

6. Conclusions

Preliminary investigation of the Endurance Basin using multibeam bathymetry and sub-bottom profiling reveals that the basin developed in a transpressional tectonic environment and sedimentation occurred by interaction of continental-slope derived instability and mass flow sedimentation with basin floor contourite sedimentation. The most recent stage of Endurance Basin development, was as a foreland basin related to thrusting of the South Georgia continental margin to the SW over lithosphere of the Central Scotia Sea. Faulting at the margins of and within the basin is consistent with left-lateral transpression.

Several sedimentary units are identified as being widely developed within the basin. Significant contourite deposits are interpreted in the northwest of the basin, as well as on the southern margin. These provide evidence of significant bottom current flow and may yield a palaeoenvironmental archive extending from present conditions to the Pliocene. Pondered units located in the central basin are interpreted as debris or density flow deposits, sourced from two different locations (the fan in the southeast of the basin and the

contourite sequence on the southern margin) and potentially governed by different causal mechanisms.

Our survey of the basin indicates its potential for obtaining high resolution palaeoenvironmental records from the northern Scotia Sea. Collection of sediment samples and additional geophysical data (notably multichannel seismics) would greatly enhance the interpretation and understanding of features and processes within the basin; which in turn may aid in understanding variation in ACC flow and climate of the South Georgia micro-continent.

Acknowledgements

We are extremely grateful for the help of Captain Jerry Burgan and the crew of the RRS James Clark Ross during cruise JR206 (NERC leg JR20100118). Julian Klepacki and Pete Lens are particularly thanked for their assistance with TOPAS troubleshooting. Elanor Gowland and Mercedes Gutierrez are thanked for their work in cleaning and gridding the archival multibeam data in the Endurance Basin area. This manuscript was significantly improved by the detailed comments of two anonymous reviewers.

Research by PTL, AJT and TJM was part of the British Antarctic Survey Polar Science for Planet Earth Programme funded by The Natural Environment Research Council. Funding for participation of Simon Day and Matthew Owen on research cruise JR206 was through a NERC-AFI-CGS grant [Instability of Submarine Volcanoes in the South Sandwich Arc CGS-11/58 (2009)] to P.T. Leat, S.J. Day and M.A. Maslin.

References

- Alendal, G., Berntsen, J., Engum, E., Furnes, G.K., Kleiven, G. and Eide, L.I., 2005. Influence from 'Ocean Weather' on near seabed currents and events at Ormen Lange. *Marine and Petroleum Geology*, 22: 21-31.
- Allen, C.S., Pike, J. and Pudsey, C.J., 2011. Last glacial-interglacial sea-ice cover in the SW Atlantic and its potential role in global deglaciation. *Quaternary Science Reviews*, 30(19-20): 2446-2458.
- Amy, L.A., Talling, P.J., Peakall, J., Wynn, R.B. and Arzola Thynne, R.G., 2005. Bed geometry used to test recognition criteria of turbidites and (sandy) debrites. *Sedimentary Geology*, 179: 163-174.

- Barker, P.F. and Burrell, J., 1977. The opening of Drake Passage. *Marine Geology*, 25: 15-34.
- Barker, P.F. and Thomas, E., 2004. Origin, signature and palaeoclimatic influence of the Antarctic Circumpolar Current. *Earth-Science Reviews*, 66: 143-162.
- Barker, P.F., 1995. Tectonic framework of the East Scotia Sea. In: B. Taylor (Editor), *Backarc Basins: Tectonics and Magmatism*. Plenum Press, New York, pp. 281-314.
- Bentley, M.J., Evans, D.J.A., Fogwill, C.J., Hansom, J.D., Sugden, D.E. and Kubik, P.W., 2007. Glacial geomorphology and chronology of deglaciation, South Georgia, sub-Antarctic. *Quaternary Science Reviews*, 26: 644-677.
- Bohoyo, F., Galindo-Zaldívar, J., Jabaloy, A., Maldonado, A., Rodríguez-Fernández, J., Schreider, A. and Suriñach, E., 2007. Extensional deformation and development of deep basins associated with the sinistral transcurrent fault zone of the Scotia Antarctic plate boundary. *Geological Society, London, Special Publications*, 290(1): 203-217.
- Bryn, P., Berg, K., Forsberg, C.F., Solheim, A. and Kvalstad, T.J., 2005a. Explaining the Storegga Slide. *Marine and Petroleum Geology*, 22(1-2): 11-19.
- Bryn, P., Berg, K., Stoker, M.S., Hafliðason, H. and Solheim, A., 2005b. Contourites and their relevance for mass wasting along the Mid-Norwegian Margin. *Marine and Petroleum Geology*, 22(1-2): 85-96.
- Canals, M., Lastras, G., Urgeles, R., Casamor, J.L., Mienert, J., Cattaneo, A., De Batist, M., Hafliðason, H., Imbo, Y., Laberg, J.S., Locat, J., Long, D., Longva, O., Masson, D.G., Sultan, N., Trincardi, F. and Bryn, P., 2004. Slope failure dynamics and impacts from seafloor and shallow sub-seafloor geophysical data: case studies from the COSTA project. *Marine Geology*, 213: 9-72.
- Casas, D., Ercilla, G., García, M., Yenes, M. and Estrada, F., 2013. Post-rift sedimentary evolution of the Gebra Debris Valley. A submarine slope failure system in the Central Bransfield Basin (Antarctica). *Marine Geology*, 340(C): 16-29.
- Civile, D., Lodolo, E., Vuan, A. and Loreto, M.F., 2012. Tectonics of the Scotia-Antarctica plate boundary constrained from seismic and seismological data. *Tectonophysics*, 550-553(C): 17-34.
- Coleman, J.M., Walker, H.J. and Grabau, W.E., 1998. Sediment instability in the Mississippi River delta. *Journal of Coastal Research*, 14(3): 872-881.

- Collins, L.G., Pike, J., Allen, C.S. and Hodgson, D.A., 2012. High-resolution reconstruction of southwest Atlantic sea-ice and its role in the carbon cycle during marine isotope stages 3 and 2. *Paleoceanography*, 27(3): PA3217.
- Cunningham, A.P., Barker, P.F. and Tomlinson, J.S., 1998. Tectonics and sedimentary environment of the North Scotia Ridge region revealed by side-scan sonar. *Journal of the Geological Society*, 155(6): 941-956.
- Dalziel, I.W.D., Dott, R.H., Winn, R.D. and Bruhn, R.L., 1975. Tectonic Relations of South Georgia Island to the Southernmost Andes. *Geological Society of America Bulletin*, 86(7): 1034-1040.
- Dalziel, I.W.D., Lawver, L.A., Norton, I.O. and Gahagan, L.M., 2013a. The Scotia Arc: genesis, evolution, global significance. *Annual Review of Earth and Planetary Sciences*, 41(1): 767-793.
- Dalziel, I.W.D., Lawver, L.A., Pearce, J.A., Barker, P.F., Hastie, A.R., Barfod, D.N., Schenke, H-W. and Davis, M.B., 2013b. A potential barrier to deep Antarctic circumpolar flow until the late Miocene? *Geology*, 41(9): 947-950.
- de Moustier, C., 2001. Field evaluation of sounding accuracy in deep water multibeam swath bathymetry. *OCEANS*, 2001. MTS/IEEE Conference and Exhibition: 1761-1765.
- Dondurur, D., Küçük, H.M. and Çifçi, G., 2013. Quaternary mass wasting on the western Black Sea margin, offshore of Amasra. *Global And Planetary Change*, 103(C): 248-260.
- Dorn, W.U. and Werner, F., 1993. The contour-current flow along the southern Iceland-Faeroe Ridge as documented by its bedforms and asymmetrical channel fillings. *Sedimentary Geology*, 82: 47-59.
- Dowdeswell, J.A., Elverhøi, A. and Spielhagen, R., 1998. Glacimarine sedimentary processes and facies on the polar North Atlantic margins. *Quaternary Science Reviews*, 17: 243-272.
- Dowdeswell, J.A., Evans, J., Ó Cofaigh, C. and Anderson, J.B., 2006. Morphology and sedimentary processes on the continental slope off Pine Island Bay, Amundsen Sea, West Antarctica. *Geological Society of America Bulletin*, 118(5-6): 606-619.
- Eagles, G., 2005. Tectonic evolution of the west Scotia Sea. *Journal of Geophysical Research*, 110(B2): B02401.
- Eagles, G., 2010. The age and origin of the central Scotia Sea. *Geophysical Journal International*, 183(2): 587-600.

- Elliott, G.M., Shannon, P.M., Houghton, P.D.W. and Øvrebø, L.K., 2010. The Rockall Bank Mass Flow: Collapse of a moated contourite drift onlapping the eastern flank of Rockall Bank, west of Ireland. *Marine and Petroleum Geology*, 27(1): 92-107.
- Faugères, J.-C. and Stow, D.A.V., 2008. Contourite drifts: nature, evolution and controls. In: M. Rebesco and A. Camerlenghi (Editors), *Contourites*. Elsevier, Amsterdam, pp. 259-288.
- Faugères, J.C., Stow, D.A.V., Imbert, P. and Viana, A., 1999. Seismic features diagnostic of contourite drifts. *Marine Geology*, 162(1): 1-38.
- Gales, J., Larter, R.D., Mitchell, N.C., Hillenbrand, C.-D., Østerhus, S. and Shoosmith, D.R., 2012. Southern Weddell Sea shelf edge geomorphology: Implications for gully formation by the overflow of high-salinity water. *Journal of Geophysical Research*, 117(F4): F04021.
- Gales, J.A., Larter, R.D., Mitchell, N.C. and Dowdeswell, J.A., 2013. Geomorphic signature of Antarctic submarine gullies: Implications for continental slope processes. *Marine Geology*, 337(C): 112-124.
- Galindo-Zaldívar, J., Jabaloy, A., Maldonado, A. and Sanz de Galdeano, C., 1996. Continental fragmentation along the South Scotia Ridge transcurrent plate boundary (NE Antarctic Peninsula). *Tectonophysics*, 258: 275-301.
- Gebbie, G. and Huybers, P., 2011. How is the ocean filled? *Geophysical Research Letters*, 38(6): L06604.
- Gersonde, R., Crosta, X., Abelmann, A. and Armand, L., 2005. Sea-surface temperature and sea ice distribution of the Southern Ocean at the EPILOG Last Glacial Maximum—a circum-Antarctic view based on siliceous microfossil records. *Quaternary Science Reviews*, 24: 869-896.
- Glicken, H., 1996. Rockslide-debris avalanche of May 18, 1980, Mount St. Helens volcano, Washington. Open-file Report 96-677, US Geological Survey.
- Goff, J.A., Kraft, B.J., Mayer, L.A., Schock, S.G., Sommerfield, C.K., Olson, H.C., Gulick, S.P. and Nordfjord, S., 2004. Seabed characterization on the New Jersey middle and outer shelf: correlatability and spatial variability of seafloor sediment properties. *Marine Geology*, 209: 147-172.
- Gordon, J.E., Haynes, V.M. and Hubbard, A., 2008. Recent glacier changes and climate trends on South Georgia. *Global and Planetary Change*, 60: 72-84.

- Graham, A.G.C., Fretwell, P.T., Larter, R.D., Hodgson, D.A., Wilson, C.K., Tate, A.J. and Morris, P., 2008. A new bathymetric compilation highlighting extensive paleo-ice sheet drainage on the continental shelf, South Georgia, sub-Antarctica. *Geochemistry Geophysics Geosystems*, 9(7): 1-21.
- Hampton, M.A., Lee, H.J. and Locat, J., 1996. Submarine landslides. *Reviews of Geophysics*, 34(1): 33-59.
- Hemming, S., 2004. Heinrich events: Massive late Pleistocene detritus layers of the North Atlantic and their global climate imprint. *Reviews of Geophysics*, 42(1): RG1005.
- Hill, I.A. and Barker, P.F., 1980. Evidence for Miocene back-arc spreading in the central Scotia Sea. *Geophysical Journal of the Royal Astronomical Society*, 63: 427-440.
- Howe, J.A., Pudsey, C.J. and Cunningham, A.P., 1997. Pliocene-Holocene contourite deposition under the Antarctic Circumpolar Current, Western Falkland Trough, South Atlantic Ocean. *Marine Geology*, 138: 27-50.
- Howe, J.A., Stoker, M.S., Masson, D.G., Pudsey, C.J., Morris, P., Larter, R.D. and Bulat, J., 2006. Seabed morphology and the bottom-current pathways around Rosemary Bank seamount, northern Rockall Trough, North Atlantic. *Marine and Petroleum Geology*, 23(2): 165-181.
- Iverson, R.M., Logan, M., Lahusen, R.G. and Berti, M., 2010. The perfect debris flow? Aggregated results from 28 large-scale experiments. *Journal of Geophysical Research*, 115(F3): F03005.
- Knutz, P.C., Jones, E.J.W., Austin, W.E.N. and van Weering, T.C.E., 2002. Glacimarine slope sedimentation, contourite drifts and bottom current pathways on the Barra Fan, UK North Atlantic margin. *Marine Geology*, 188: 129-146.
- Knutz, P.C., Zahn, R. and Hall, I.R., 2007. Centennial-scale variability of the British Ice Sheet: Implications for climate forcing and Atlantic meridional overturning circulation during the last deglaciation. *Paleoceanography*, 22(1): 14.
- Laberg, J.S. and Vorren, T.O., 2000. Trænadjupet slide, offshore Norway - morphology, evacuation and triggering mechanisms. *Marine Geology*, 171: 95-114.
- Laberg, J.S., Vorren, T.O., Mienert, J., Evans, D., Lindberg, B., Ottesen, D., Kenyon, N.H. and Henriksen, S., 2002. Late Quaternary palaeoenvironment and chronology in the Trænadjupet Slide area offshore Norway. *Marine Geology*, 188: 35-60.

- Larter, R.D., Vanneste, L.E., Morris, P. and Smyth, D.K., 2003. Structure and tectonic evolution of the South Sandwich arc. In: R.D. Larter and P.T. Leat (Editors), *Intra-Oceanic Subduction Systems: Tectonic and Magmatic Processes*. Geological Society, London, Special Publications 219, pp. 255-284.
- Leat, P.T., Tate, A.J., Deen, T.J., Day, S.J. and Owen, M.J., 2010. RRS James Clark Ross JR206 cruise report: volcanic and continental slope processes, South Georgia and South Sandwich Islands. British Antarctic Survey Cruise Report ES6/1/2010/1.
- Livermore, R., Hillenbrand, C.-D., Meredith, M. and Eagles, G., 2007. Drake Passage and Cenozoic climate: An open and shut case? *Geochemistry Geophysics Geosystems*, 8(1): Q01005.
- Livermore, R., McAdoo, D. and Marks, K., 1994. Scotia Sea tectonics from high-resolution satellite gravity. *Earth and Planetary Science Letters*, 123: 255-268.
- Llave, E., Schönflied, J., Hernández-Molina, F.J., Mulder, T., Somoza, L., Díaz del Río, V. and Sánchez-Almazo, I., 2006. High-resolution stratigraphy of the Mediterranean outflow contourite system in the Gulf of Cadiz during the late Pleistocene: The impact of Heinrich events. *Marine Geology*, 227: 241-262.
- Lobo, F., Hernández-Molina, F., Bohoyo, F., Galindo-Zaldívar, J., Maldonado, A., Martos, Y., Rodríguez-Fernández, J., Somoza, L. and Vázquez, J., 2011. Furrows in the southern Scan Basin, Antarctica: interplay between tectonic and oceanographic influences. *Geo-Marine Letters*, 31(5-6): 451-464.
- Lodolo, E., Civile, D., Vuan, A., Tassone, A. and Geletti, R., 2010. The Scotia-Antarctica plate boundary from 35°W to 45°W. *Earth and Planetary Science Letters*, 293(1-2): 200-215.
- Lodolo, E., Donda, F. and Tassone, A., 2006. Western Scotia Sea margins: Improved constraints on the opening of the Drake Passage. *Journal of Geophysical Research*, 111(B6): B06101.
- Maldonado, A., Barnolas, A., Bohoyo, F., Escutia, C., Galindo-Zaldívar, J., Hernández-Molina, J., Jabaloy, A., Lobo, F., Hans Nelson, C., Rodríguez-Fernández, J., Somoza, L. and Vázquez, J., 2005. Miocene to Recent contourite drifts development in the northern Weddell Sea (Antarctica). *Global and Planetary Change*, 45: 99-129.
- Maldonado, A., Barnolas, A., Bohoyo, F., Galindo-Zaldívar, J., Hernández-Molina, J., Lobo, F., Rodríguez-Fernández, J., Somoza, L. and Vázquez, J., 2003. Contourite

deposits in the central Scotia Sea: the importance of the Antarctic Circumpolar Current and the Weddell Gyre flows. *Palaeogeography, Palaeoclimatology, Palaeoecology*, 198: 187-221.

Mann, P., Draper, G. and Lewis, J.F., 1991. An overview of the geologic and tectonic development of Hispaniola. *Geological Society of America Special Papers*, 262: 1-28.

Marani, M., Argnani, A., Roveri, M. and Trincardi, F., 1993. Sediment drifts and erosional surfaces in the central Mediterranean: seismic evidence of bottom-current activity. *Sedimentary Geology*, 82: 207-220.

McCave, I.N., Manighetti, B. and Beveridge, N.A.S., 1995. Circulation in the glacial North-Atlantic inferred from grain-size measurements. *Nature*, 374(6518): 149-152.

Meredith, M., Watkins, J., Murphy, E., Ward, P., Bone, D., Thorpe, S., Grant, S. and Ladkin, R., 2003. Southern ACC Front to the northeast of South Georgia: Pathways, characteristics, and fluxes. *Journal of Geophysical Research*, 108(C5): 3162.

Meredith, M.P., Garabato, A.C.N., Gordon, A.L. and Johnson, G.C., 2008. Evolution of the Deep and Bottom Waters of the Scotia Sea, Southern Ocean, during 1995 - 2005. *Journal of Climate*, 21(13): 3327-3343.

Mulder, T. and Alexander, J., 2001. The physical character of subaqueous sedimentary density flows and their deposits. *Sedimentology*, 48: 269-299.

Mulder, T., Syvitski, J., Migeon, S., Faugères, J.C. and Savoye, B., 2003. Marine hyperpycnal flows: initiation, behavior and related deposits. A review. *Marine and Petroleum Geology*, 20: 861-882.

Noormets, R., Dowdeswell, J.A., Larter, R.D., Ó Cofaigh, C. and Evans, J., 2009. Morphology of the upper continental slope in the Bellingshausen and Amundsen Seas - Implications for sedimentary processes at the shelf edge of West Antarctica. *Marine Geology*, 258(1-4): 100-114.

Orsi, A., Johnson, G. and Bullister, J., 1999. Circulation, mixing, and production of Antarctic Bottom Water. *Progress in Oceanography*, 43: 55-109.

Orsi, A., Whitworth III, T. and Nowlin Jr, W., 1995. On the meridional extent and fronts of the Antarctic Circumpolar Current. *Deep-Sea Research Part I*, 42(5): 641-673.

Øvrebø, L.K., Haughton, P.D.W. and Shannon, P.M., 2006. A record of fluctuating bottom currents on the slopes west of the Porcupine Bank, offshore Ireland - implications for Late Quaternary climate forcing. *Marine Geology*, 225(1-4): 279-309.

- Owen, M., Day, S. and Maslin, M., 2007. Late Pleistocene submarine mass movements: occurrence and causes. *Quaternary Science Reviews*, 26(7-8): 958-978.
- Pelayo, A.M. and Wiens, D.A., 1989. Seismotectonics and relative plate motions in the Scotia Sea region. *Journal of Geophysical Research*, 94(B6): 7293-7320.
- Piper, D.J.W., Hiscott, R.N. and Normark, W.R., 1999. Outcrop-scale acoustic facies analysis and latest Quaternary development of Hueneme and Dume submarine fans, offshore California. *Sedimentology*, 46: 47-78.
- Preu, B., Hernández-Molina, F.J., Violante, R., Piola, A.R., Marcelo Paterlini, C., Schwenk, T., Voigt, I., Krastel, S. and Spiess, V., 2013. Morphosedimentary and hydrographic features of the northern Argentine margin The interplay between erosive, depositional and gravitational processes and its conceptual implications. *Deep-Sea Research Part I*, 75(c): 157-174.
- Pubellier, M., Mauffret, A., Leroy, S., Vila, J.M. and Amilcar, H., 2000. Plate boundary readjustment in oblique convergence: Example of the Neogene of Hispaniola, Greater Antilles. *Tectonics*, 19(4): 630-648.
- Pudsey, C.J. and Howe, J.A., 1998. Quaternary history of the Antarctic Circumpolar Current: evidence from the Scotia Sea. *Marine Geology*, 148: 83-112.
- Pudsey, C.J. and Howe, J.A., 2002. Mixed biosiliceous-terrigenous sedimentation under the Antarctic Circumpolar Current, Scotia Sea. *Geological Society, London, Memoirs*, 22(1): 325-336.
- Rosqvist, G.C. and Schuber, P., 2003. Millennial-scale climate changes on South Georgia, Southern Ocean. *Quaternary Research*, 59: 470-475.
- Rothwell, R.G., Thomson, J. and Kähler, G., 1998. Low-sea-level emplacement of a very large Late Pleistocene 'megaturbidite' in the western Mediterranean Sea. *Nature*, 392: 377-380.
- Schlesinger, A., Cullen, J., Spence, G., Hyndman, R., Loudon, K. and Mosher, D., 2012. Seismic velocities on the Nova Scotian margin to estimate gas hydrate and free gas concentrations. *Marine and Petroleum Geology*, 35(1): 105-115.
- Smalley Jr., R., Dalziel, I.W.D., Bevis, M.G., Kendrick, E., Stamps, D.S., King, E.C., Taylor, F.W., Lauría, E., Zakrajsek, A. and Parra, H., 2007. Scotia arc kinematics from GPS geodesy. *Geophysical Research Letters*, 34(21): L21308.

- Smith, I.J., Stevens, D.P., Heywood, K.J. and Meredith, M.P., 2009. The flow of the Antarctic Circumpolar Current over the North Scotia Ridge. *Deep-Sea Research Part I*, 57(1): 14-28.
- Solheim, A., Bryn, P., Sejrup, H.P., Mienert, J. and Berg, K., 2005. Ormen Lange - an integrated study for the safe development of a deep-water gas field within the Storegga Slide Complex, NE Atlantic continental margin; executive summary. *Marine and Petroleum Geology*, 22(1-2): 1-9.
- Stow, D.A.V. and Faugères, J.-C., 2008. Contourite facies and the facies model. In: M. Rebesco and A. Camerlenghi (Editors), *Contourites*. Elsevier, Amsterdam, pp. 223-255.
- Sugden, D.E. and Clapperton, C.M., 1977. The Maximum Ice Extent on Island Groups in the Scotia Sea, Antarctica. *Quaternary Research*, 7: 268-282.
- Talling, P.J., Masson, D.G., Sumner, E.J. and Malgesini, G., 2012. Subaqueous sediment density flows: Depositional processes and deposit types. *Sedimentology*, 59(7): 1937-2003.
- Tate, A.J. and Leat, P.T., 2007. RRS James Clark Ross JR168 cruise report: swath bathymetry South Sandwich Islands. *British Antarctic Survey Cruise Report ES6/1/2007/1*. 16pp.
- Thomas, C., Livermore, R. and Pollitz, F., 2003. Motion of the Scotia Sea plates. *Geophysical Journal International*, 155: 789-804.
- Thorpe, S.E., Heywood, K.J., Brandon, M.A. and Stevens, D.P., 2002. Variability of the southern Antarctic Circumpolar Current front north of South Georgia. *Journal Of Marine Systems*, 37(1-3): 87-105.
- Tripsanas, E.K., Piper, D.J.W. and Campbell, D.C., 2008. Evolution and depositional structure of earthquake-induced mass movements and gravity flows: Southwest Orphan Basin, Labrador Sea. *Marine and Petroleum Geology*, 25(7): 645-662.
- Tripsanas, E.K., Piper, D.J.W., Jenner, K.A. and Bryant, W.R., 2007. Submarine mass-transport facies: new perspectives on flow processes from cores on the eastern North American margin. *Sedimentology*, 55(0): 97-136.
- USGS, 2014. Significant Earthquake Archive, <http://earthquake.usgs.gov/earthquakes/search/>. Accessed 06/03/2014.
- Van der Putten, N., Verbruggen, C., Ochyra, R., Spassov, S., de Beaulieu, J., De Dapper, M., Hus, J. and Thouveny, N., 2009. Peat bank growth, Holocene palaeoecology and

climate history of South Georgia (sub-Antarctica), based on a botanical macrofossil record. *Quaternary Science Reviews*, 28(1-2): 65-79.

Voigt, I., Henrich, R., Preu, B.M., Piola, A.R., Hanebuth, T.J., Schwenk, T. and Chiessi, C.M., 2013. A submarine canyon as a climate archive - Interaction of the Antarctic Intermediate Water with the Mar del Plata Canyon (Southwest Atlantic). *Marine Geology*, 341(C): 46-57.

Volpi, V., Camerlenghi, A., Hillenbrand, C.-D., Rebesco, M. and Ivaldi, R., 2003. Effects of biogenic silica on sediment compaction and slope stability on the Pacific margin of the Antarctic Peninsula. *Basin Research*, 15: 339-363.

Walsh, J.P., Corbett, D.R., Mallinson, D., Goni, M., Dail, M., Loewy, C., Marciniak, K., Ryan, K., Smith, C., Stevens, A., Sumners, B. and Tesi, T., 2006. Mississippi Delta mudflow activity and 2005 Gulf hurricanes. *EOS*, 87(44): 477-479.

Whitworth III, T. and Nowlin Jr, W., 1987. Water masses and currents of the Southern Ocean at the Greenwich Meridian. *Journal of Geophysical Research*, 92(C6): 6462-6476.

Zachos, J., Pagani, M., Sloan, L., Thomas, E. and Billups, K., 2001. Trends, Rhythms, and Aberrations in Global Climate 65 Ma to Present. *Science*, 292(5517): 686-693.

Figure Captions

Figure 1: Regional map of Scotia Sea. A. Tectonic setting, thick black lines indicate key tectonic plate boundaries, solid inset box shows location of Figure 2. B. Present-day oceanographic setting, current circulation from Maldonado et al. (2003) and frontal locations from Meredith et al. (2003). SAF - Subantarctic Front; PF - Polar front; SACCF - Southern Antarctic Current Front; SB - Southern boundary of Antarctic Circumpolar Current; SRP - Shag Rocks Passage. C. South Georgia microcontinent and seismicity from USGS (2014).

Figure 2: Detailed bathymetric map of Endurance Basin also showing location of TOPAS lines and subsequent figures in this paper. Figure location is shown in Figure 1. Some interpreted features are also shown: scarps are interpreted as faults (see Figure 13 and section 5 for discussion). Scarps A - C are shown in Figure 3.

Figure 3: Bathymetry and interpretative figures of mass transport scarps from the northeast margin of Endurance Basin, locations of scarps shown on Figure 2. Scarps are interpreted as faults (see Figure 13 and section 5 for discussion).

Figure 4: JR206 TOPAS line 17, northwest to southeast transect part 1. A. Location of profile. B. TOPAS data shown with 30 x vertical exaggeration. C. Interpreted section, dashed boxes indicate location of Figures 5.A and 5.B.

Figure 5: High resolution image of sub-surface features shown in TOPAS line 17. A. TOPAS line 17 inset box 1. B. TOPAS line 17 inset box 2.

Figure 6: JR206 TOPAS line 7, northwest to southeast transect part 2. A. Location of profile. B. TOPAS data shown with 25 x vertical exaggeration. C. Interpreted section, dashed boxes indicate location of Figures 7.A and 7.B.

Figure 7: High resolution image of sub-surface features shown in TOPAS line 7. A. TOPAS line 7 inset box 1. B. TOPAS line 7 inset box 2.

Figure 8: JR206 TOPAS line 12, northwest to southeast transect part 3. A. Location of profile. B. TOPAS data shown with 25 x vertical exaggeration. C. Interpreted section.

Figure 9: JR206 TOPAS line 11, south to north transect. A. Location of profile. B. TOPAS data shown with 25 x vertical exaggeration. C. Interpreted section.

Figure 10: JR206 TOPAS line 9, example of interpreted contourite deposit from Endurance Basin's southern margin. A. Location of profile. B. TOPAS data shown with 25 x vertical exaggeration. C. Interpreted section.

Figure 11: Overview of interpreted seismic units.

Figure 12: Isopach of seismic units III and IV. A. Isopach of Unit IV. B. Isopach of Unit III. Thin black lines show location of TOPAS profiles interpreted, thicknesses calculated using an assumed seismic velocity of 1600 m s^{-1} . Data plotted with bathymetric shaded relief; location indicated on Figure 2.

Figure 13: Interpreted processes and features within Endurance Basin. A. Structural. B. Sedimentation and ocean circulation pathways.

Table captions

Table 1: Data used in this study.

Table 2: Overview of TOPAS lines.

Table 3: Morphological characteristics of Endurance Basin.

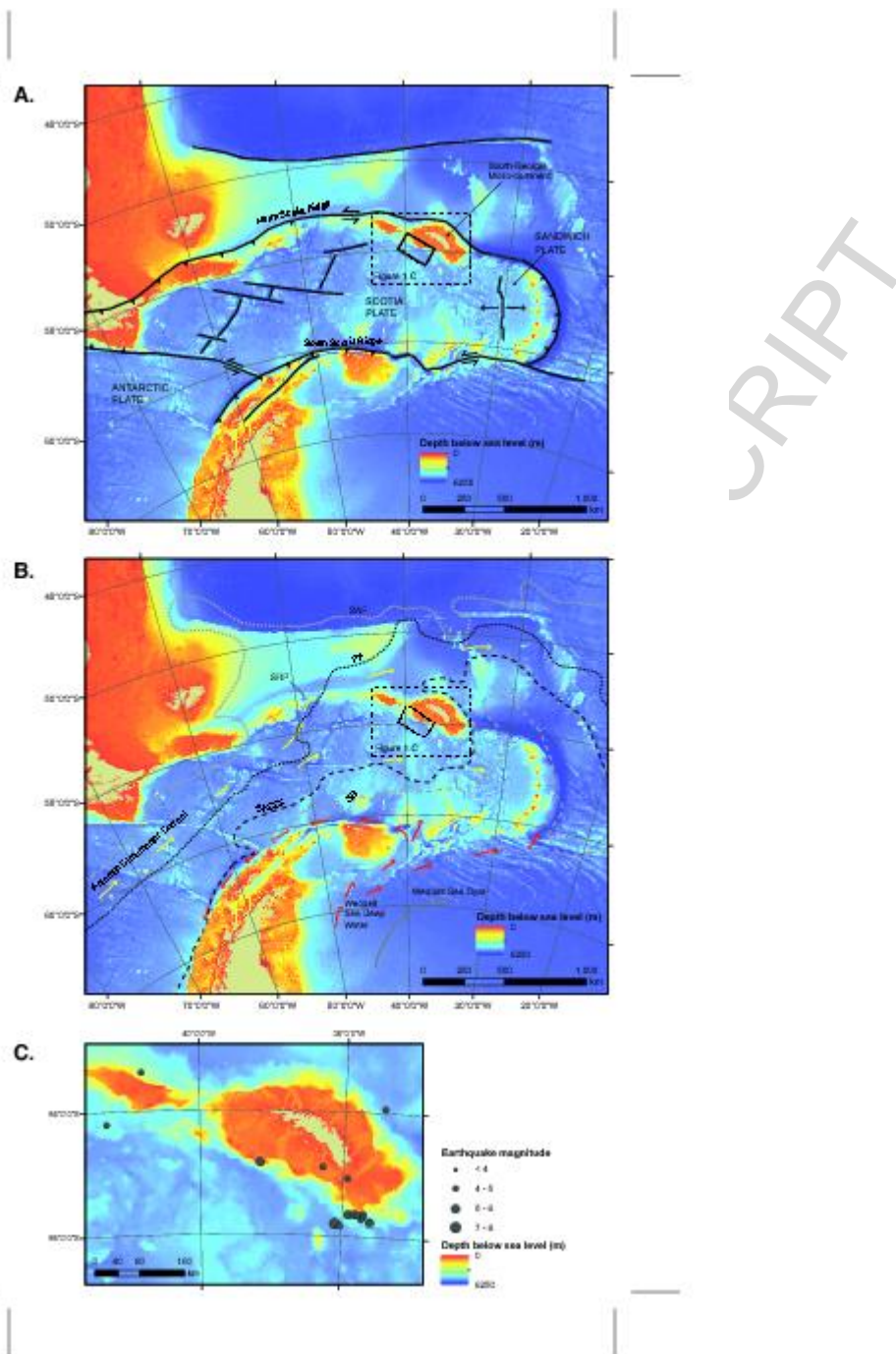


Figure 1

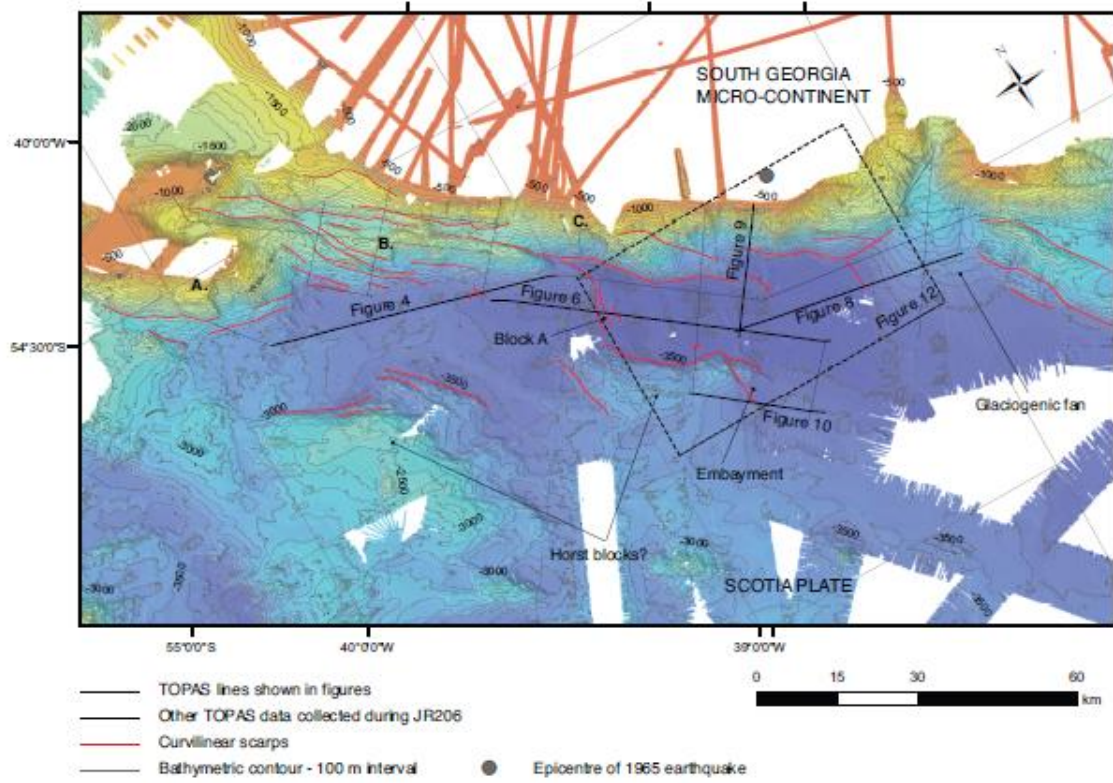


Figure 2

ACCEPTED

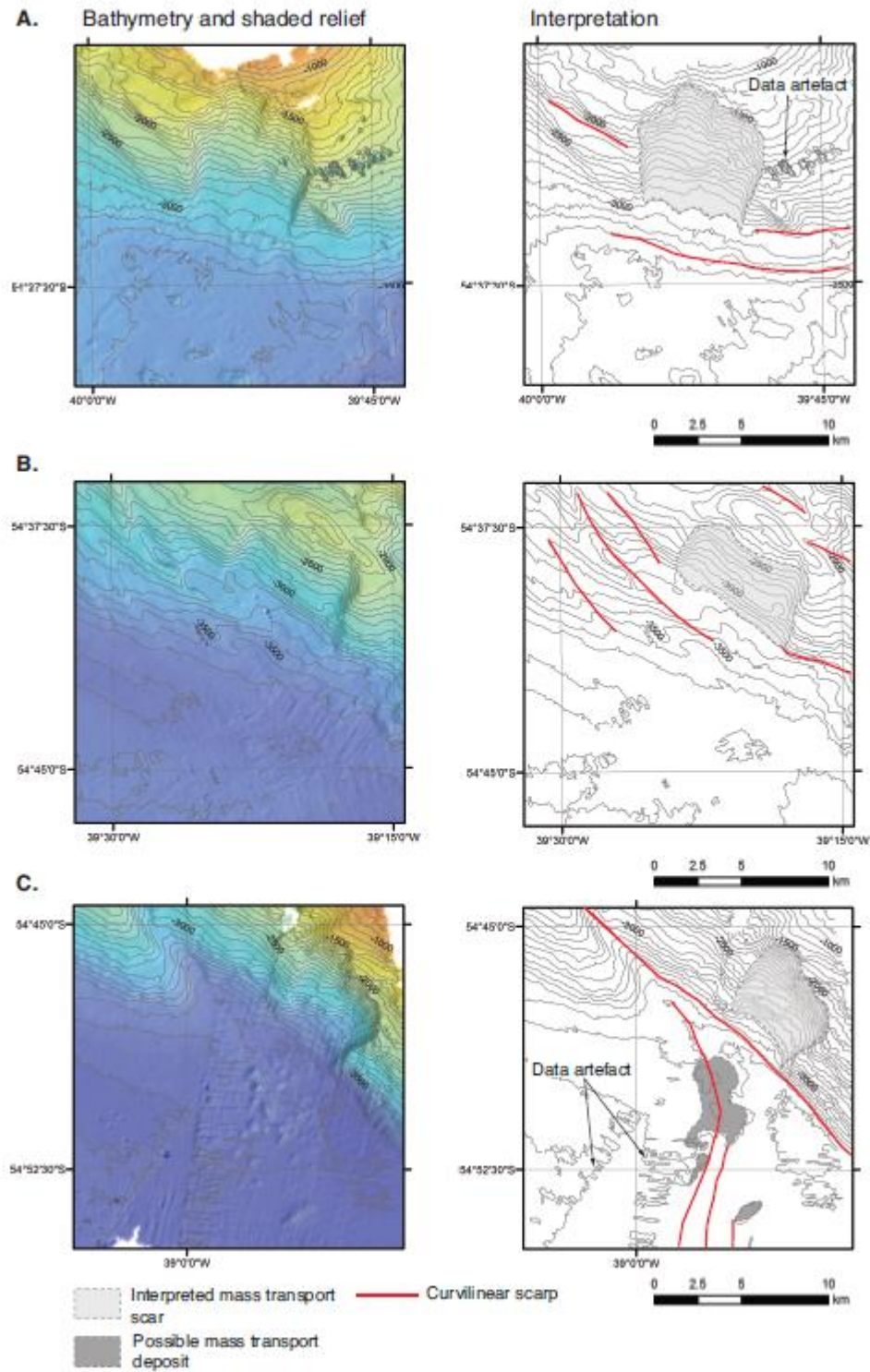


Figure 3

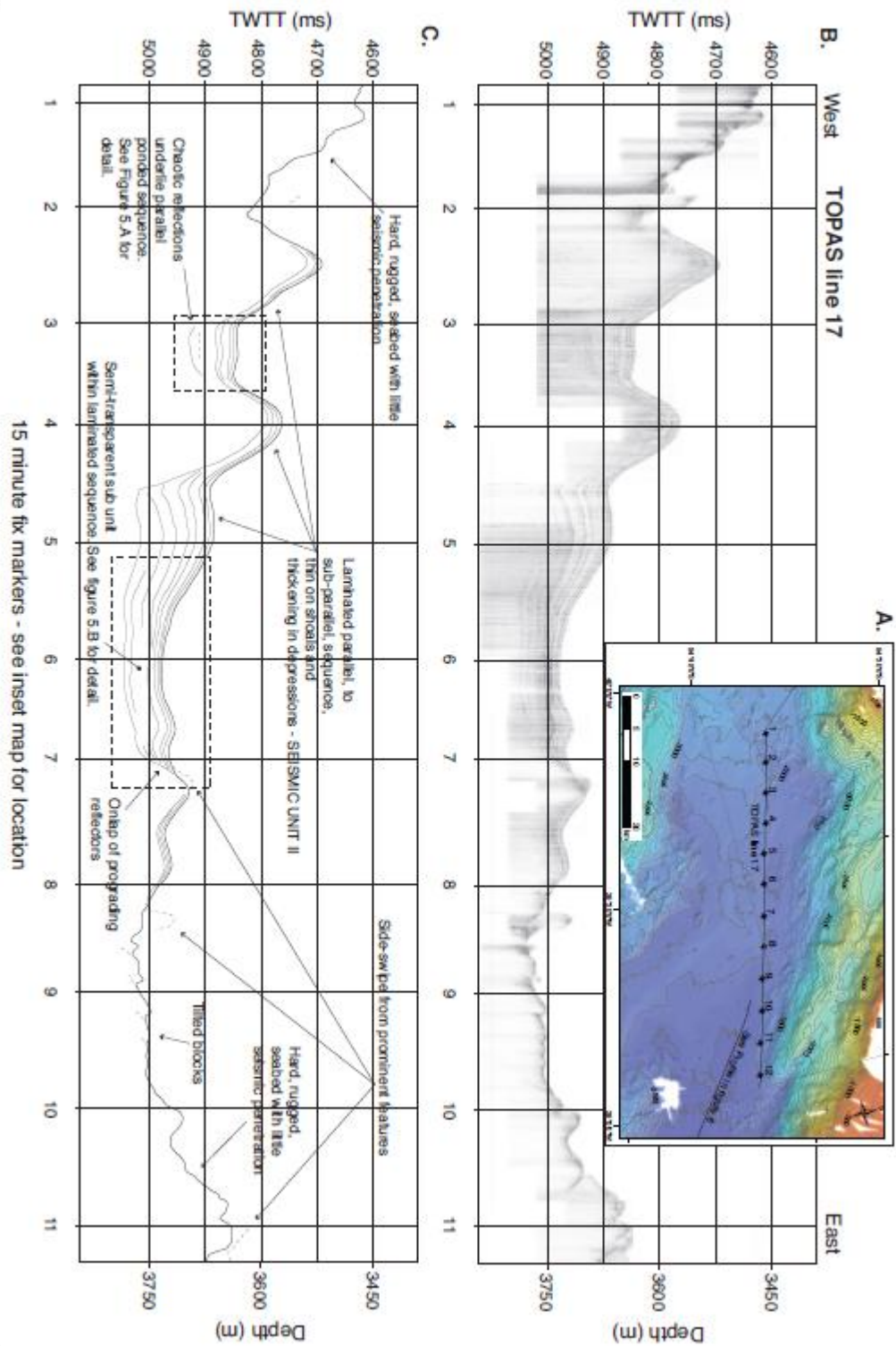
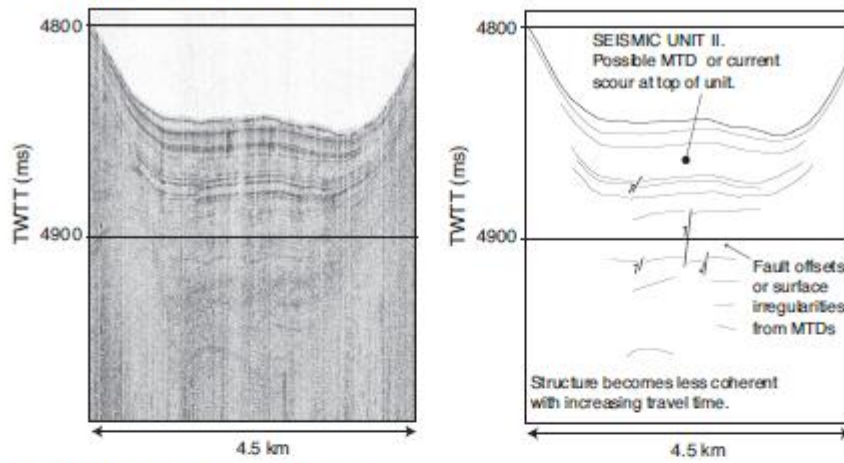


Figure 4

A. TOPAS line 17 - inset box 1



B. TOPAS line 17 - inset box 2

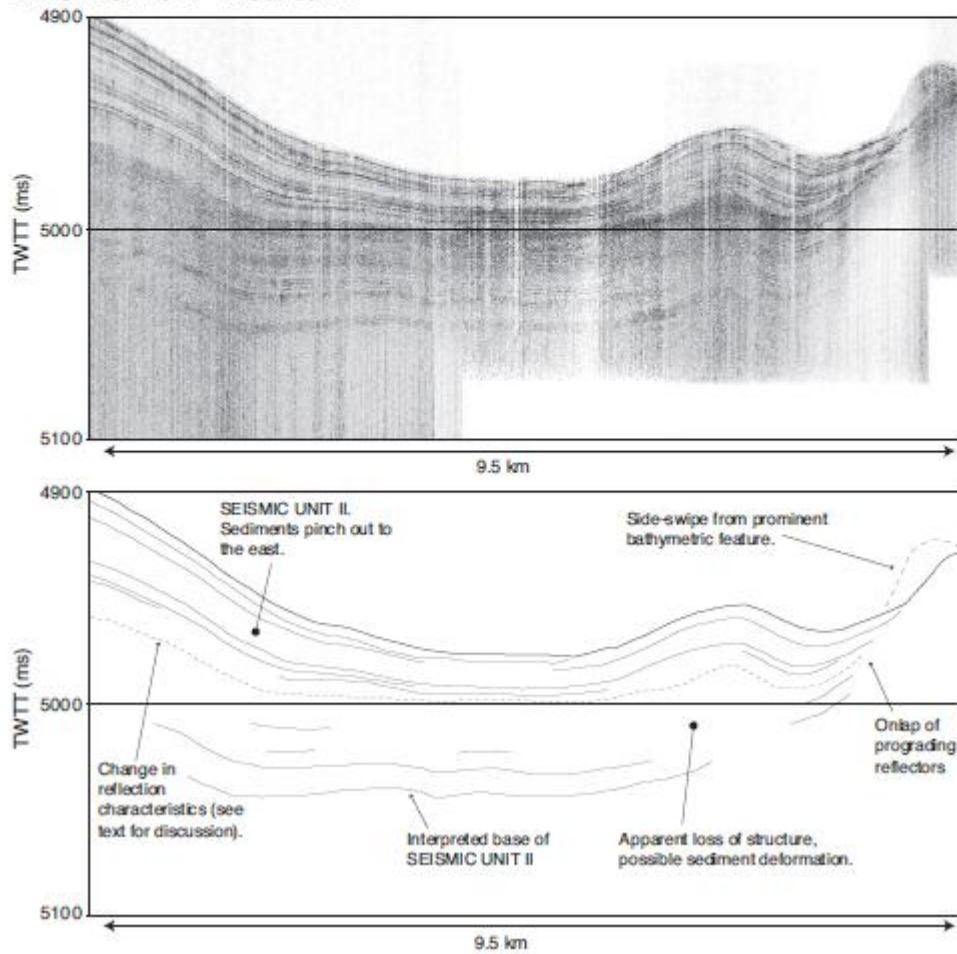


Figure 5

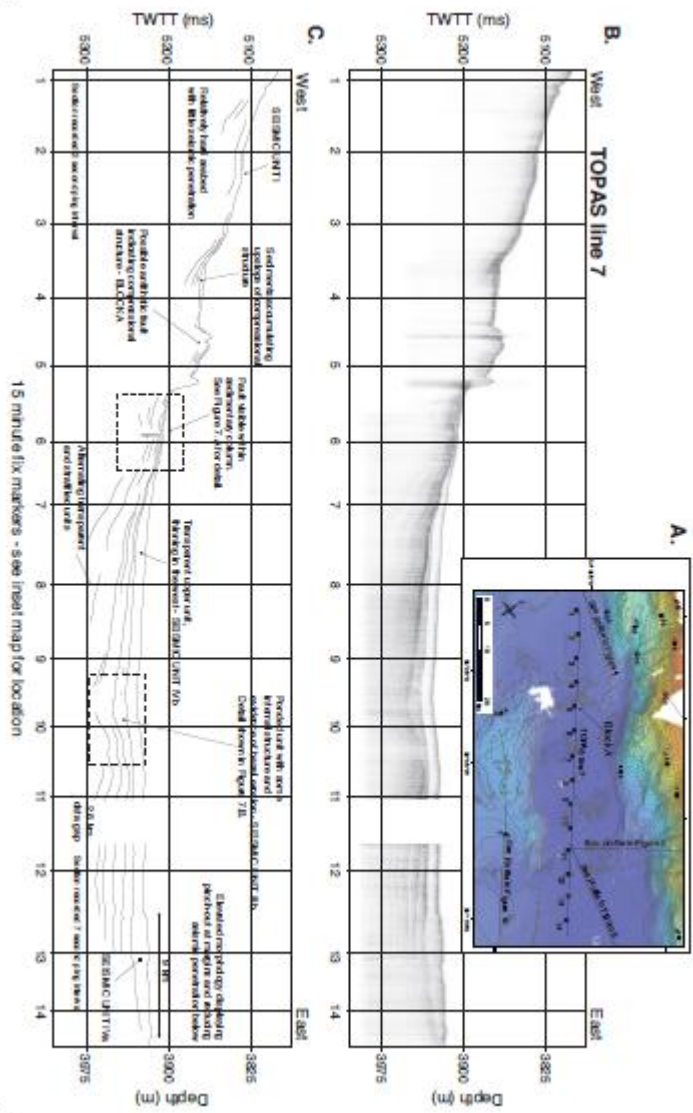


Figure 6

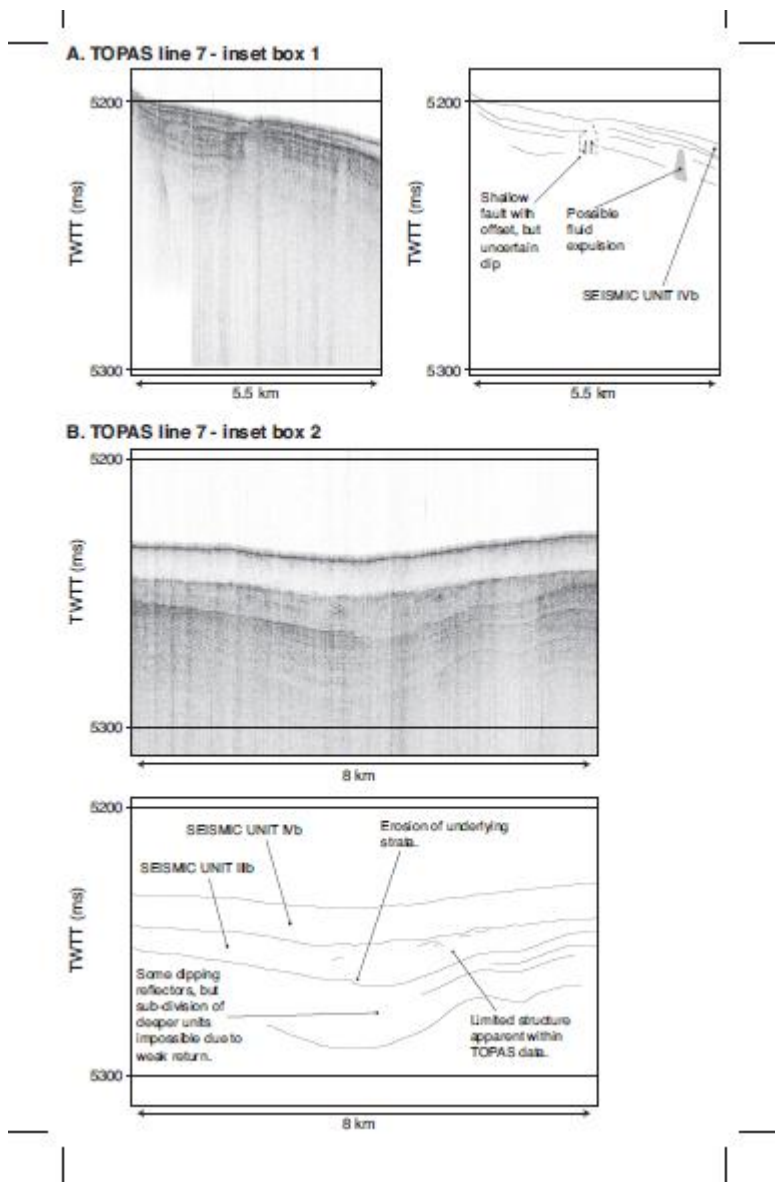


Figure 7

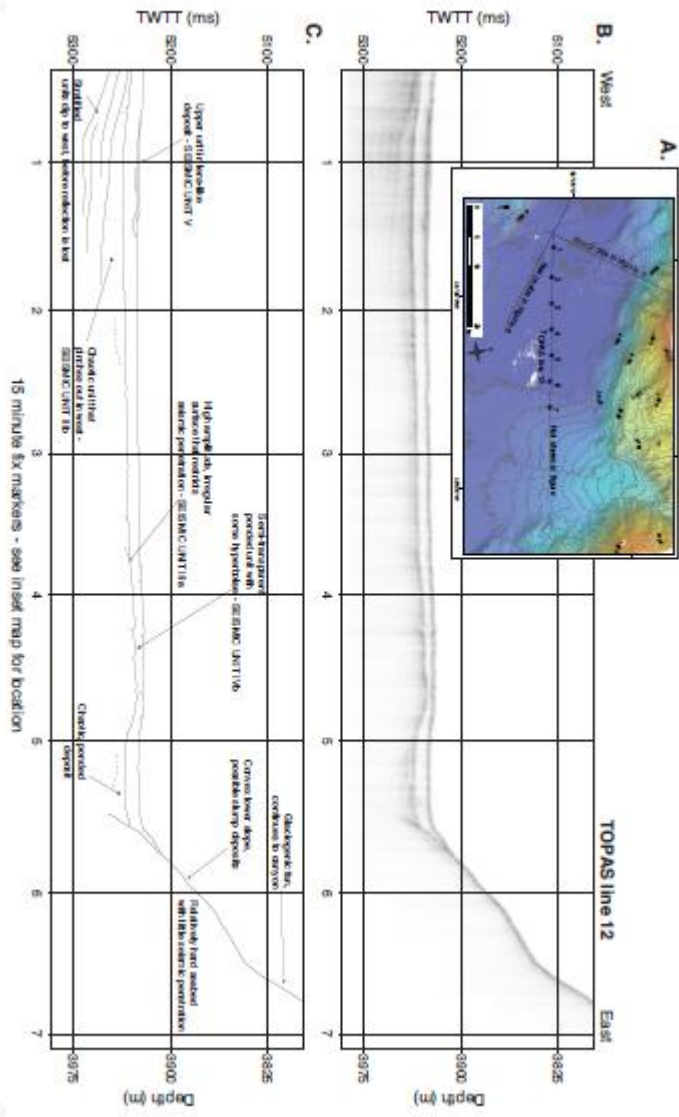


Figure 8

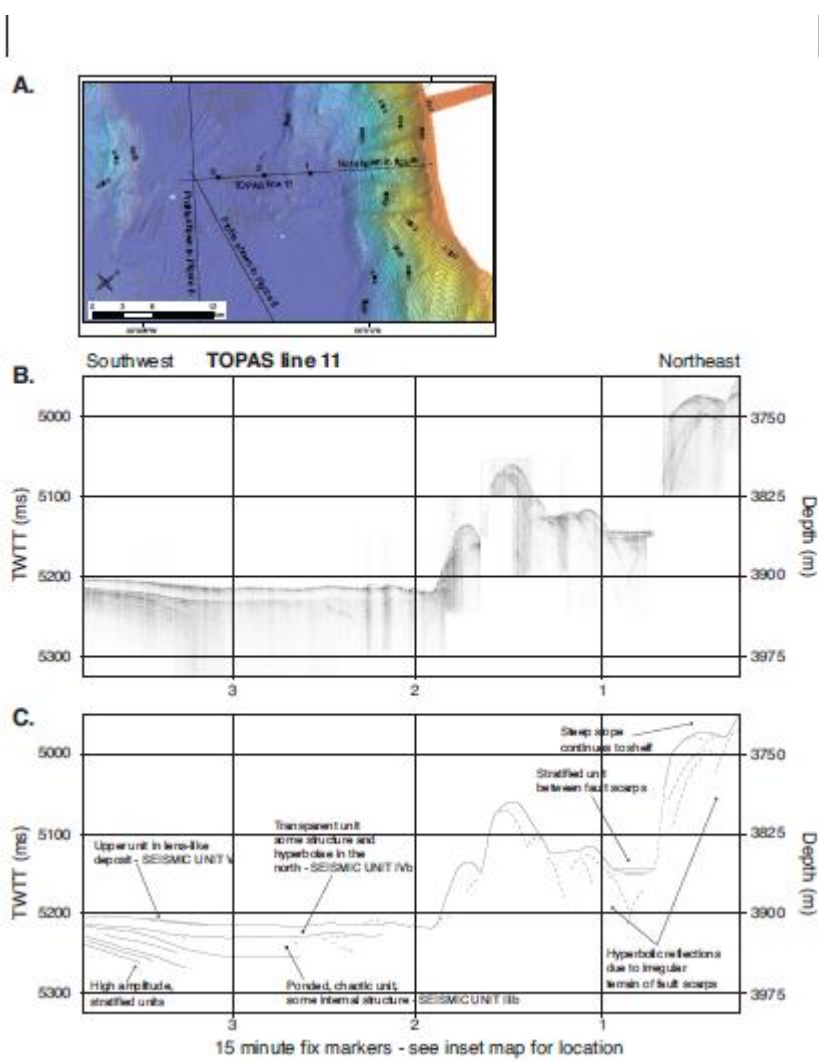


Figure 9

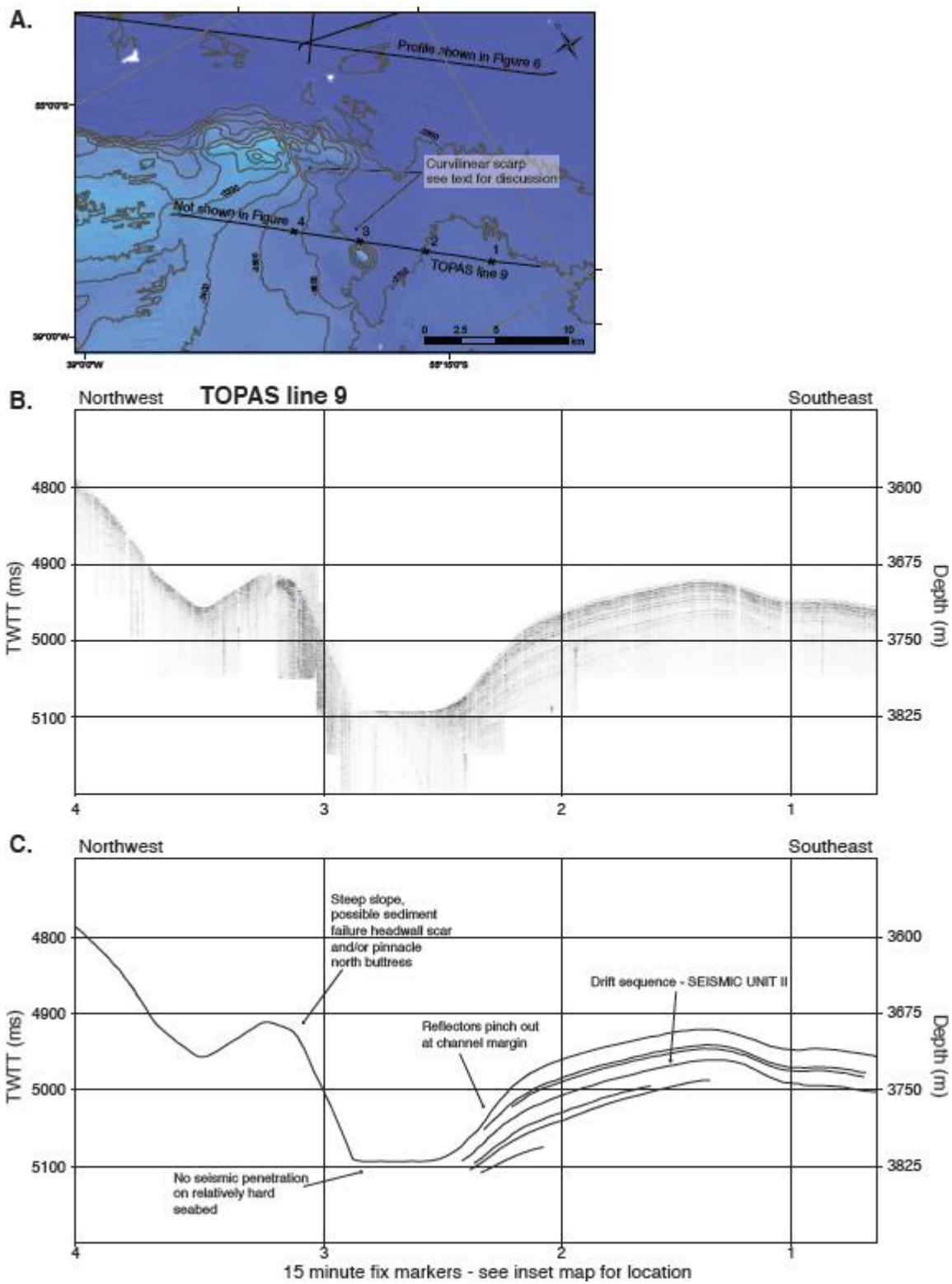


Figure 10

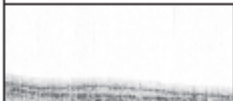
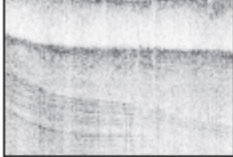
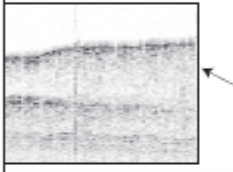
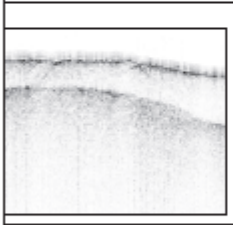
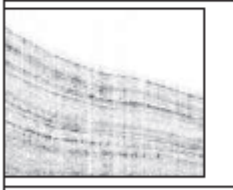
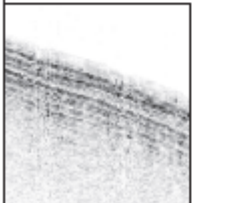
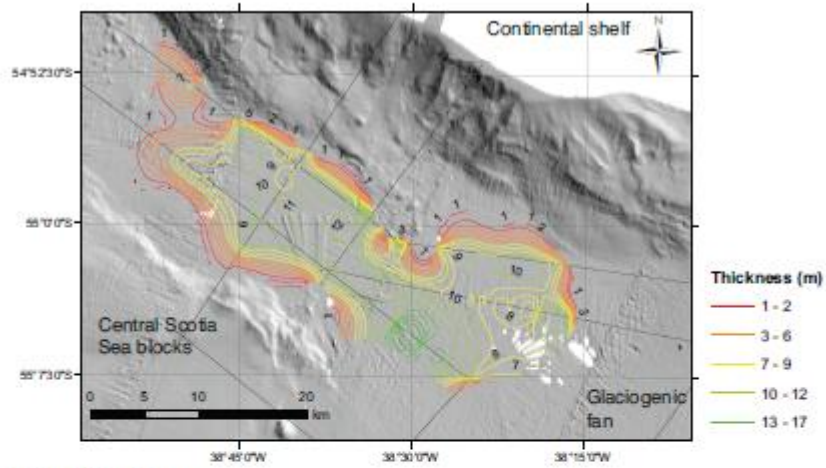
TOPAS data example	Identifying Characteristics	Seismic Unit
	Transparent, lens-like surface unit (Figures 8 and 9)	Unit V
	Semi-transparent, slightly ponded unit (see Figures 6 and 8).	Unit IVb
	Chaotic, high amplitude, ponded unit. Base of unit is erosive at times (see Figures 6, 7 and 8).	Unit IIIb
	Irregular, elevated upper surface morphology associated with the semi-transparent, slightly ponded unit (see Figure 6). Refers to upper section of data example.	Unit IVa
	Elevated morphology associated with the chaotic, high amplitude, ponded unit. Acts as a barrier to TOPAS penetration (see Figure 8). Refers to buried surface in data example.	Unit IIIa
	Parallel to sub-parallel laminated sequence, relatively low amplitude with significant seismic penetration (see sequences interpreted in Figures 4 and 10).	Unit II
	Stratified parallel reflectors of generally high amplitude, with limited seismic penetration (see western section of Figure 6).	Unit I

Figure 11

A. Unit IV thickness



B. Unit III thickness

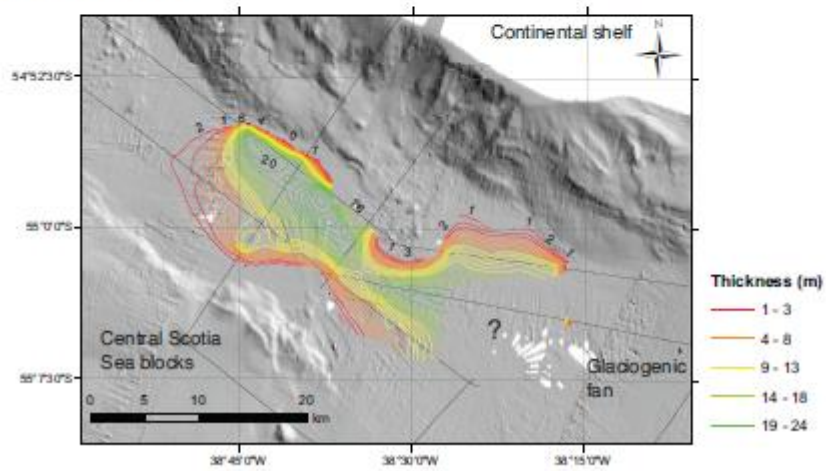


Figure 12

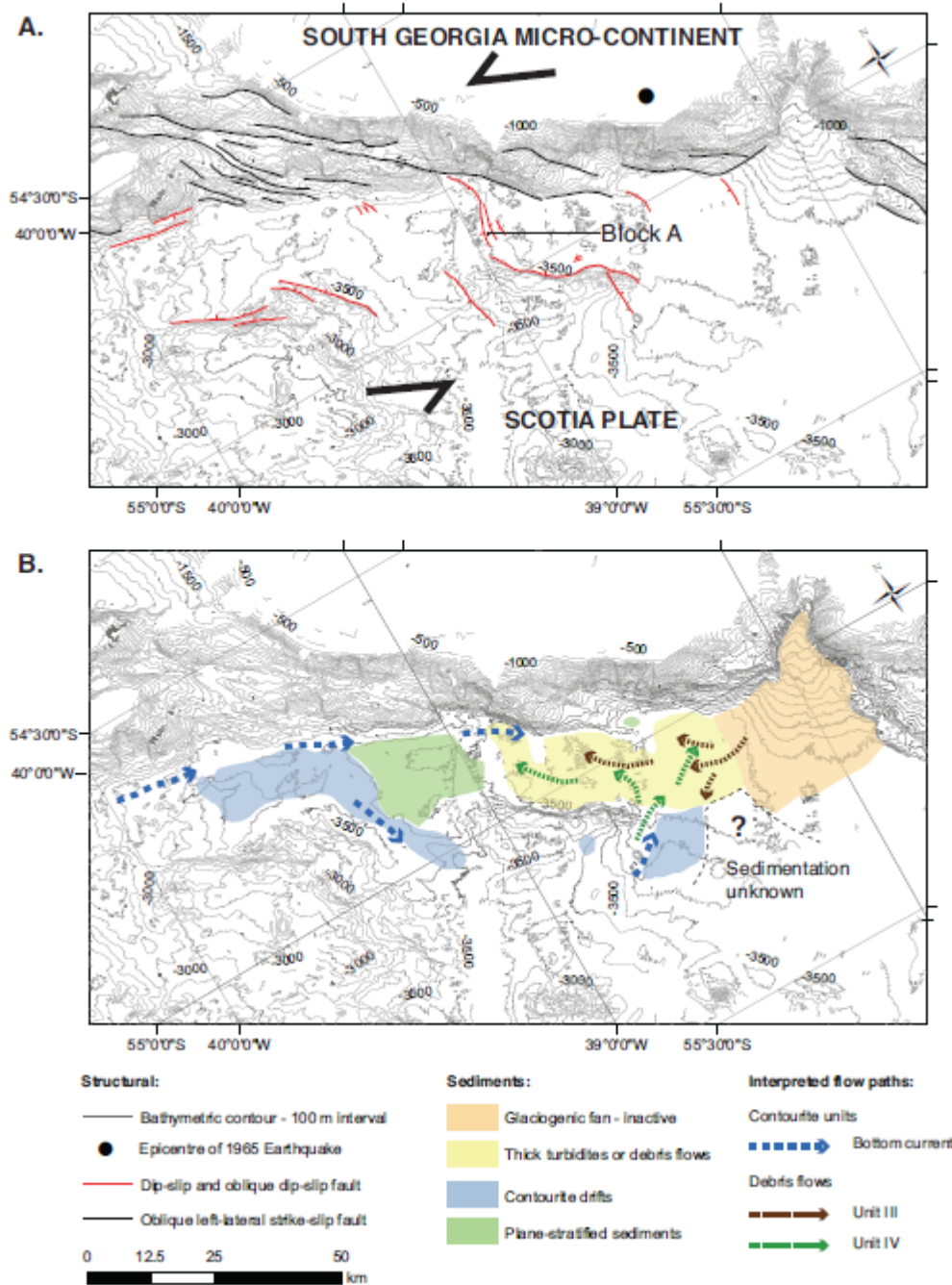


Figure 13

Table 1

Data type	Summary
JR206 Bathymetry	Acquired from RRS James Clark Ross with Simrad EM120 multibeam echosounder.
JR206 TOPAS	667 km of data acquired from RRS James Clark Ross with Simrad TOPAS PS 018 (Details shown in Table 2).
Additional bathymetry	Data previously acquired by RRS James Clark Ross (17 cruises). Primarily acquired on passage, with the exception of an area in the southeast where a block of data was acquired during cruise JR103.

Bathymetric grid, the underlying source data and the TOPAS data are available from the Polar Data Centre, hosted by the British Antarctic Survey.

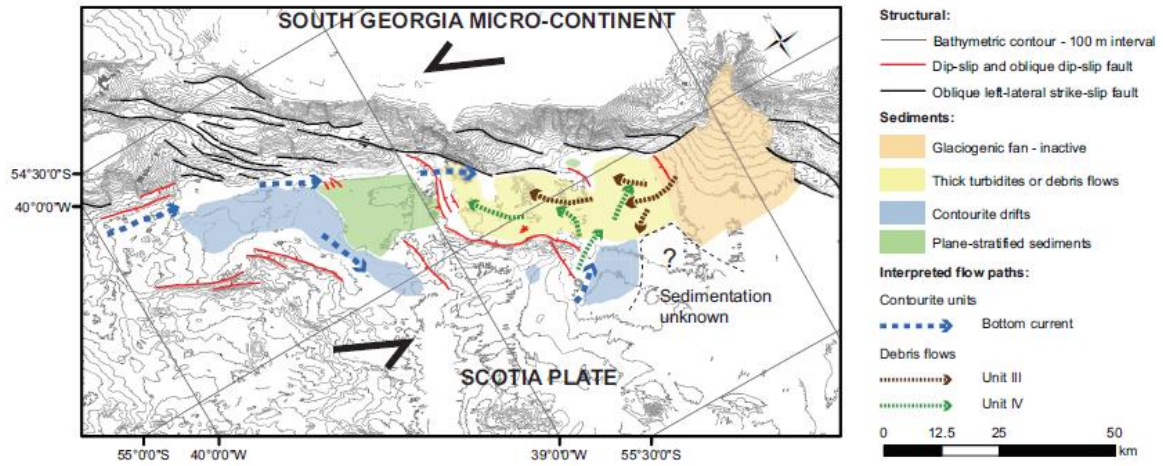
ACCEPTED MAN

Table 2

Line Name	Latitude - Start (D.D)	Longitude - Start (D.D)	Latitude - End (D.D)	Longitude - End (D.D)	Vessel speed (kts)	Ping interval (ms)	Line length (km)
JR206_TOPAS_01	-54.3645	-39.8489	-54.7213	-39.1316	10	External	64.2
JR206_TOPAS_02	-54.6863	-39.0753	-54.5059	-39.4890	10	External	33.4
JR206_TOPAS_03	-54.5053	-39.4833	-54.5441	-39.5439	6	1250-2000	16.5
JR206_TOPAS_03a	-54.6165	-39.6323	-54.6801	-39.5006	6	2000	11.1
JR206_TOPAS_04	-54.6772	-39.5113	-54.5374	-39.2935	6	2000	21.1
JR206_TOPAS_06	-54.7816	-39.2341	-54.6457	-39.0278	6	2000	20.2
JR206_TOPAS_07	-54.7928	-39.1918	-55.1310	-38.4037	10	2000-7000	61.6
JR206_TOPAS_08	-55.1267	-38.4122	-55.2273	-38.5679	10	7000	15.0
JR206_TOPAS_09	-55.2316	-38.5219	-55.0899	-38.8408	10	7000	25.7
JR206_TOPAS_10	-55.0993	-38.8371	-54.8269	-38.5230	10 – 6	7000-2000	36.4
JR206_TOPAS_11	-54.8686	-38.4032	-55.0501	-38.6308	6 – 10	2000	24.9
JR206_TOPAS_12	-55.0377	-38.6288	-55.1112	-37.9394	10	2000	44.8
JR206_TOPAS_13	-55.1079	-37.9496	-55.0450	-37.8698	6	2000	8.7
JR206_TOPAS_14	-55.0469	-37.8729	-55.0012	-38.0592	6	2000	13.0
JR206_TOPAS_14a	-54.9972	-38.0468	-54.9454	-37.8782	10	2000	12.2
JR206_TOPAS_15	-54.9455	-37.8793	-55.2005	-38.1723	6 – 10	2000	34.0
JR206_TOPAS_16	-54.5745	-39.9506	-54.6656	-39.8253	10	2000	13.0
JR206_TOPAS_17	-54.6659	-39.8243	-54.8057	-39.0075	10	2000	54.9
JR206_TOPAS_18	-54.9062	-39.0062	-55.0155	-38.5114	10	2000	33.9
JR206_TOPAS_19	-55.0155	-38.5114	-55.0667	-37.8488	10	2000	42.7
JR206_TOPAS_20	-55.0667	-37.8488	-55.2111	-37.5091	10	2000	27.0
JR206_TOPAS_21	-55.2114	-37.5080	-55.3529	-36.7085	12	External	53.2
Total							667.4

Table 3

Region	Feature characteristics					
Endurance Basin - overview	Length:	140 km	Width:	15 - 30 km	Area:	2630 km ²
	Maximum water depth:	3930 m	Mean water depth:	3709 m	Gradient along basin axis - west to east:	0.5°
Northern margin	Relief:	3300 m	Typical Gradient:	13°	Maximum gradient:	49°
Southern margin	Relief:	500 - 1100 m	Typical Gradient:	13° on steep slopes, 2° on more gently angled embayments	Maximum gradient:	35°
Western sub-basin	Length:	74 km	Width:	15 - 26 km	Area:	1355 km ²
	Maximum water depth:	3830 m	Mean water depth:	3603 m	Gradient along basin axis - west to east:	0.5°
Eastern sub-basin	Length:	50 km	Width:	23 - 12 km	Area:	695 km ²
	Maximum water depth:	3930 m	Mean water depth:	3875 m	Gradient along basin axis - west to east:	0.2°
Glaciogenic fan	Length:	39 km	Width:	32 km	Area:	629 km ²
	Water depth at summit:	2550 m	Water depth at toe:	3850 m	Typical Gradient:	2.5°



Graphical abstract

ACCEPTED MANUSCRIPT

Highlights

- Endurance Basin is adjacent to South Georgia's southern continental margin
- It is around 160 km long and 20 - 50 km wide and consists of at least three sub-basins
- Bathymetry provides evidence of transpression with oblique strike-slip faults
- TOPAS data reveals debris flows accumulating in the central basin
- Contourite units may contain a palaeoenvironmental archive extending to the Pliocene

ACCEPTED MANUSCRIPT